Analysis of secondary inorganic aerosols over the Greater Area of Athens using the EPISODE-CityChem source dispersion and photochemistry model

Stelios Myriokefalitakis[1], Matthias Karl[2], Kim A. Weiss[1,3], Dimitris Karagiannis[1], Eleni Athanasopoulou[1], Anastasia Kakouri[1], Aikaterini Bougiatioti[1], Eleni Liakakou[1], Iasonas Stavroulas[1], Georgios Papangelis[1], Georgios Grivas[1], Despina Paraskevopoulou[1], Orestis Speyer[1], Nikolaos Mihalopoulos[1], and Evangelos Gerasopoulos[1]

[1] Institute for Environmental Research and Sustainable Development (IERSD), National Observatory of Athens, Penteli, Greece

[2] Helmholtz-Zentrum Hereon GmbH, Geesthacht, Germany

[3] Natural Sciences, Institute of Physics and Meteorology, Earth and Climate System Sciences, Universität Hohenheim, Stuttgart, Germany

Correspondence to: Stelios Myriokefalitakis (steliosm@noa.gr) and Matthias Karl (matthias.karl@hereon.de)

Abstract. Secondary inorganic aerosols (SIA) are major components of fine particulate matter (PM$_{2.5}$), having substantial implications for climate and air quality in an urban environment. In this study, a state-of-the-art thermodynamic model has been coupled to the source dispersion and photochemistry city-scale chemistry transport model EPISODE-CityChem, able to simulate pollutants on a horizontal resolution of 100 x 100 m^2, to determine the equilibrium between the inorganic gas and aerosol phases over the Greater Area of Athens, Greece, for the year 2019. In agreement with in-situ observations, sulfate (SO$_4^{2-}$) is calculated to have the highest annual mean surface concentration (2.15 ± 0.88 µg m^{-3}) among SIA in the model domain, followed by ammonium (NH$_4^+$; 0.58 ± 0.14 µg m^{-3}) and fine nitrate (NO$_3^-$; 0.24 ± 0.22 µg m^{-3}). Simulations denote that NO$_3^-$ formation strongly depends on the local nitrogen oxide emissions, along with the ambient temperature, the relative humidity, and the photochemical activity. Additionally, we show that anthropogenic combustion sources may have an important impact on the NO$_3^-$ formation in an urban area. During the cold period, the combined effect of decreased temperature in the presence of non-sea salt potassium favors the partitioning of HNO$_3$ in the aerosol phase in the model, raising the NO$_3^-$ formation in the area. Overall, this work highlights the significance of atmospheric composition and the local meteorological conditions for the equilibrium distribution of nitrogen-containing semivolatile compounds and the acidity of inorganic aerosols, especially in urban areas where atmospheric trace elements from natural and anthropogenic sources coexist.

1 Introduction

Fine particulate matter ($PM_{2.5}$) impacts the planet's radiative balance (Myhre et al., 2014) and severely affects air quality (WHO, 2021). Such effects strongly depend on the chemical and physical properties of $PM_{2.5}$, e.g., shape, size distribution, and hygroscopicity. Among other particulate pollutants, like organic matter, elemental carbon, dust particles, and sea spray, secondary inorganic aerosols (SIAs) are identified as a critical $PM_{2.5}$ fraction in an urban atmosphere. SIAs are formed in the atmosphere via gas-to-particle conversion of precursors of anthropogenic (e.g., coal combustion, biomass burning, vehicular), biomass burning, and natural (e.g., marine, soil, lightning, volcanoes) origin, with sulfate (SO_4^{2-}), nitrate (NO_3^-), and ammonium (NH_4^+) being the three major SIA species. However, primary emissions, such as those from residential combustion, have been found to increase their atmospheric abundance (Zhang et al., 2023). SIAs may further contribute significantly to air quality degradation; for example, sulfates can reduce visibility and contribute to acid rain (Liu et al., 2019), affecting forest and aquatic ecosystems (Driscoll et al., 2003, 2016), and damaging building materials (Ozga et al., 2013). On the other hand, SIAs are also linked to increased asthma exacerbation (Sarnat et al., 2015) and cardiovascular hospitalization (Basagaña et al., 2015) and can contribute to human mortality via the enhancement of fine particulate air pollution (Franklin et al., 2008; Pope et al., 2020). Focusing, in particular, on polluted environments, Nenes et al. (2020) indicated that atmospheric acidity, aerosol liquid water content (LWC), and meteorological conditions (temperature and relative humidity) are the main parameters that control SIA formation sensitivity, depending on ammonia (NH_3) and nitric acid (HNO_3) availability.

Sulfates are primarily formed by the oxidation of sulfur dioxide (SO_2) as a byproduct of fossil fuel burning, such as coal and oil in power plants and industrial processes, as well as residual oil burning in shipping. In the gas phase, the SO_2 homogeneous oxidation via OH radicals during daytime strongly depends on temperature, while the heterogeneous oxidation of SO_2 via H_2O_2/O_3 may proceed in aqueous media such as cloud liquid water and in-cloud scavenging processes (Seinfeld and Pandis, 2006), enhanced in the presence of transition metal ions (e.g., Mn^{2+} and Fe^{3+}; Alexander et al., 2009), and/or on aerosol surfaces such as dust aerosols (Wang et al., 2022). Aqueous phase processes are nevertheless found to be responsible for about two-thirds of the total sulfate production in the global troposphere (e.g., Myriokefalitakis et al., 2022). Overall, it is well established that the amounts of precursor gases and oxidants, the cloud cover, the amount of available surface area, and meteorological factors such as temperature and relative humidity all affect the rate of SO_2 conversion to sulfate (Liu et al., 2021).

Particulate nitrate formation depends on the emissions of nitrogen oxides (NO_X) from traffic, power plants, and industrial activities, along with the gas-phase concentrations of ammonia (NH_3) as emitted by agricultural activities, waste management, industrial processes, and the biosphere. The formation of NO_3^- is, however, a rather complex process, strongly dependent on interactions of acidity, relative humidity, and temperature (Guo et al., 2017b; Nenes et al., 2020), with the partitioning of HNO_3 to the particulate phase enhanced under lower ambient temperatures (Guo et al., 2017b). Nevertheless, since ammonium nitrate (NH_4NO_3) is formed when NH_3 is in excess upon the formation of ammonium sulfate and ammonium bisulfate, such an equilibrium, besides the availability of NH_3, also depends on the concentration of sulfuric acid (H_2SO_4). The relative humidity is, nevertheless, a key factor for SIA formation, determining the aerosol LWC and thus the aerosol acidity levels, which in

62 turn impact the HNO₃ partitioning in the aerosol phase. All in all, NO_3^- formation increases the aerosol LWC by lowering

63 aerosol acidity via dilution and thus further promoting HNO₃ partitioning into the particulate phase (Guo et al., 2017a).

64 Thermodynamic calculations (Clegg et al., 1998; Fountoukis and Nenes, 2007; Nenes et al., 1998) are considered to be the

65 appropriate way of assessing non-linearities in an inorganic aerosol system and the behavior of a non-ideal liquid solution.

66 Such methods can explicitly account for the equilibrium state of inorganic particles by calculating the gas- and particulate-

67 phase fractions of the inorganics, along with the corresponding aerosol LWC and the respective levels of acidity (pH), both of

68 which are very important for assessing the burden of the secondary inorganic PM fraction. The presence of nonvolatile cations

69 (NVCs) in thermodynamic calculations, however, has been shown to substantially affect the ion balance (Guo et al., 2018) and

70 thus the partitioning of HNO_3/NO_3^- and NH_3/NH_4^+ species, especially in areas with abundant mineral dust and sea spray

71 aerosols (Athanasopoulou et al., 2008, 2016), such as the Eastern Mediterranean. For example, calcium-containing dust

72 particles may react with nitric acid to form calcium nitrate ($Ca(NO_3)_2$), significantly enhancing NO_3^- formation, especially

73 when natural and anthropogenic particulate matter coexist. On the other hand, NVCs from combustion sources related to

74 natural or anthropogenic activities may also critically impact the predictions of inorganic partitioning between the gas and the

75 particulate phase in an urban environment (Cheng et al., 2022).

76 Regional chemistry transport models (CTM) are promising tools for providing spatial information on environmental impacts

77 occurring in the urban landscape. Although such modeling tools can successfully simulate the inorganic and organic

78 components of atmospheric aerosols at the background scale (e.g., Brandt et al., 2003; Athanasopoulou et al., 2013; Zakoura

79 and Pandis, 2018; Basla et al., 2022), they are not rather accurate in the representation of their spatial distribution in proximity

80 to point and/or line sources (Santiago et al., 2022). On the contrary, urban-scale CTM models have the

81 advantage of mapping air pollution levels in high-resolution (≤ 1km) (e.g., Hurley et al., 2005;

82 Karl et al., 2019; Denby et al., 2020), although critical processes related to air quality, such as aerosol representation and its

83 chemical speciation, may still be simplistically represented due to the high computational load of such modeling systems.

84 Indeed, urban-scale CTMs usually estimate the bulk mass of particulate matter ($PM_{2.5}$ and/or PM_{10}) without having

85 incorporated their chemical interactions with gaseous pollutants in the atmosphere, like in the case of inorganic chemical

86 components in the aqueous and/or solid state. Such a simplistic aerosol parameterization in local/city-scale models, which still

87 remains a common approach, nevertheless represents the next challenging issue of multi-scale modeling (Sokhi et al., 2022).

88 Several regional-scale numerical simulations of atmospheric pollution have been performed over the Eastern Mediterranean

89 area (Athanasopoulou et al., 2015; Fountoukis et al., 2011; Im et al., 2013; Kontos et al., 2021; Kushta et al., 2019; Liora et

90 al., 2022), focusing in particular on the urban area of Athens, one of the most polluted cities in the EU. Most of these studies

91 highlight the complex interactions among nitrogen and sulfur oxides of anthropogenic origin with sea salt and/or dust particles

92 of natural origin over the area (Athanasopoulou et al., 2008; Karydis et al., 2016). These findings are also confirmed by several

93 local observational studies (Bardouki et al., 2003; Dimitriou et al., 2021; Koçak et al., 2004, 2012; Stavroulas et al., 2021). On

94 the other hand, recent city-scale modeling studies over Athens (Gratsea et al., 2021; Grivas et al., 2020; Lasne et al., 2023;

3

95 Ramacher et al., 2021) clearly demonstrate the difficulties in simulating the inorganic constituents of atmospheric aerosols in

96 the area, in particular at the intra-urban scale.

97 To tackle the above challenges in the context of multi-pollutant studies at a city-scale spatial resolution, we here develop a

98 framework for fine aerosol thermodynamic calculations to better understand the SIA formation mechanisms in an urban

99 environment. Section 2 provides an overview of the model, focusing mostly on the new developments applied in this study. In

00 particular, we describe the aqueous-phase chemistry scheme used to simulate the atmospheric SO_4^{2-} production in cloud

01 droplets, the respective developments for the thermodynamic calculations of semi-volatile inorganics, along with a series of

02 code updates currently applied in the model. In Sect. 3, we present the model-derived SO_4^{2-}, NO_3^-, and NH_4^+ surface

03 concentrations and their evaluation against in situ observations. Finally, in Sect. 4, we discuss the simulated processes and

04 summarize the implications of explicitly resolving the secondary formation of $PM_{2.5}$ in a city-scale chemistry transport model

05 for air quality, as well as the plans for future model development.

06 **2. Methodology and Data**

07 The numerical atmospheric model system used for this study is the chemistry-transport model (CTM) EPISODE-CityChem

08 (Karl et al., 2019), coupled here to atmospheric processes relevant to SIA formation. The model is applied over the Greater

09 Area of Athens (Greece), centered at the urban center (Fig. 1), horizontally covering a domain of 45 x 45 km^2 (SW corner

10 23.4E°, 37.8N°, 1 x 1 km^2 cell size, with a subgrid of 100 m) and vertically representing a 24-layered atmosphere up to 3.7

11 km. For the current study, simulations of air quality are performed for 2019. Three simulations have been conducted in this

12 work to investigate uncertainties regarding the impact of SIA formation in the Greater Area of Athens (GAA): i) the base

13 simulation where a complete chemistry/thermodynamic scheme is accounted in the model (W/ SIA); ii) a simulation where

14 the secondary production of SO_4^{2-}, NO_3^-, and NH_4^+ is neglected (W/O SIA), that is focused on the impact of long-range

15 transport to SIA concentrations in the study area; and iii) an extra simulation where the impact of NVC emissions related to

16 domestic burning on the SIA formation is neglected (W/O Kbb), focusing thus on the importance of potassium (K$^+$) on the

17 equilibrium distribution of nitrogen-containing semivolatile compounds. Finally, available in situ measurements for the area

18 and year of study are used to assess the accuracy of model predictions and the efficiency of the performed advancements.

19 **2.1 The EPISODE-CityChem model**

20 EPISODE-CityChem is a city-scale CTM designed for treating complex atmospheric chemistry in urban areas and improving

21 the representation of near-field dispersion. EPISODE is an Eulerian dispersion model developed by the Norwegian Institute

22 for Air Research (Slørdal et al., 2007) to simulate pollutant dispersion at the city scale and microscale simultaneously.

23 EPISODE consists of a 3-D Eulerian grid that interacts with a subgrid Gaussian dispersion model for the dispersion of

24 pollutants emitted from both line and point sources (Hamer et al., 2020), allowing the retrieval of pollutant concentrations at

25 the subgrid scale in an urban area. The CityChem extension offers an explicit description of the gaseous reactive pollutants

26 photochemistry on the Eulerian grid, along with the dispersion close to point emission sources (e.g., industrial stacks) and line
27 emission sources (open roads and streets). For this work, however, supplementary emissions are incorporated into the model
28 domain (see Sect. 2.1.3) to enable a realistic simulation of SIA formation.

29 **2.1.1 Gas-phase chemistry**

30 EPISODE-CityChem has several schemes for solving the chemistry of the gas phase. For the standard model configuration,
31 the updated chemistry scheme, EmChem09-HET, is applied on the coarse grid, which supports more than 100 reactions,
32 including photodissociation, thermal, and heterogeneous reactions, and about 70 species. However, for this study, the well-
33 documented Carbon Bond Mechanism 2005 (CB05; Yarwood et al., 2005), along with more recent modifications (mCB05) as
34 introduced by Williams et al. (2013, 2017) are applied. For comparison, we note that the mCB05 configuration here uses 50
35 tracers with roughly 134 reactions, respectively. The Kinetic PreProcessor (KPP) software version 2.2.3 (Damian et al., 2002;
36 Sandu and Sander, 2006) is employed to integrate the mCB05 gas-phase chemical mechanism for this work, based on the
37 generated Rosenbrock solver. A more detailed description and evaluation of the mCB05-KPP implementation can be found in
38 Myriokefalitakis et al. (2020).

39 Photodissociation rates were calculated inline using the Tropospheric Ultraviolet and Visible (TUV) Radiation model (Lee-
40 Taylor and Madronich, 2002). The TUV module calculates actinic flux and photolysis rates in each vertical layer within a 1-
41 D column of the Eulerian grid. The implemented wavelength grid ranges from 170-735 nm with 138 wavelength bins; 31
42 photodissociation reactions (out of 113 available in TUV) were selected for the implemented TUV module, covering all
43 relevant photolysis rates in the lower troposphere. Additionally, the model includes a light-dependent ground surface source
44 of nitrous acid (HONO) on top of the respective direct emissions from vehicles (Karl and Ramacher, 2021). In more detail, the
45 ground surface reaction producing HONO was parameterized according to Zhang et al. (2016) with a NO uptake coefficient
46 (gamma) depending on the light intensity, i.e., when light intensity is less than 400 W m^{-2} a gamma value of 2×10^{-5} is used;
47 otherwise, a factor of light intensity/400 is used to scale the gamma value.

48 Pollutant concentrations in the sub-grid components (i.e., the Gaussian models for line and point source dispersion) are
49 determined by the EP10-Plume scheme, which contains 10 compounds and 17 reactions of O_3, NO, NO_2, HNO_3, CO, and
50 formaldehyde (HCHO). In the line source sub-grid model, the simplified street canyon model (SSCM) is applied to calculate
51 pollutant dispersion in street canyons, and in the point source sub-grid model, the WMPP (WORM Meteorological Pre-
52 Processor) is integrated to calculate the wind speed at plume height. The rate of change of the concentrations of NO, NO_2, and
53 O_3 in a street canyon is described in terms of chemical reaction, direct emissions, and background concentration. The mixing
54 processes are parameterized via the mixing time, which corresponds to the typical residence time of pollutants in a street
55 canyon. More details on the sub-grid photochemistry schemes of EPISODE-CityChem can be found in (Karl et al., 2019).

2.1.2 Extensions to the aerosol scheme

EPISODE-CityChem is extended for this work with online calculations of the main inorganic aerosol components, SO_4^{2-}, NO_3^-, and NH_4^+, in the presence of non-volatile cations from sea salt, dust, and domestic heating. For this, the aqueous-phase formation of SO_4^{2-} in cloud droplets and the thermodynamic calculations, which determine the gas/particle partitioning of NH_3/NH_4^+ and HNO_3/NO_3^-, are explicitly considered in the model. Aqueous phase oxidation of the dissolved SO_2 via H_2O_2 and O_3 in cloud droplets is added to the model. H_2O_2 produced in the gas phase can be rapidly dissolved in the liquid phase due to its high solubility, and the dissolved H_2O_2 reacts rapidly with the HSO_3^-. Note that the dissociation of H_2O_2 is neglected here. SO_2 oxidation in the aqueous phase is much faster than its gas phase homogeneous oxidation via OH radicals, with the dissolved H_2O_2 being the most effective oxidant in the aqueous phase (Seinfeld and Pandis, 2006), especially when the solution becomes acidic. At a higher pH (pH > 4), the dissolved SO_2 oxidation by ozone (O_3) tends to dominate the S(IV) oxidation, even under dark conditions. Although laboratory studies have shown that dissolved SO_2 can also be oxidized in the presence of transition metals via other pathways (Harris et al., 2013), such reactions are not currently considered in our model. Lastly, the acidity of clouds is calculated using the electro-neutrality of strong acids (i.e., H_2SO_4, SO_4^{2-}, HNO_3, NO_3^-) and NH_4^+, along with the dissociations of CO_2, SO_2, and NH_3. The reaction rates and the constants used to calculate the sulfur chemistry in the model are presented in Table 1.

The ISORROPIA II thermodynamic equilibrium model (Fountoukis and Nenes, 2007) has been coupled to EPISODE-CityChem to calculate the gas/particle partitioning of inorganic aerosols. ISORROPIA-II calculates the gas–liquid–solid equilibrium partitioning of the K^+ - Ca^{2+} - Mg^{2+} - NH_4^+ - Na^+ - SO_4^{2-} - NO_3^- - Cl^- - H_2O aerosol system, and it is applied here in the forward mode. NVCs from dust and sea salt aerosols are taken into account in the thermodynamic calculations considered here as a fraction of $PM_{2.5}$ concentration. It is here assumed that constant mass ratios correspond to dust concentrations for Ca^{2+}, Na^+, K^+, and Mg^{2+} of 1.2%, 1.5%, and 0.9%, respectively (Sposito, 1989). Accordingly, for sea spray aerosols, mean mass fractions of 55.0% Cl^-, 30.6% Na^+, 7.7% SO_4^{2-}, 3.7% Mg^{2+}, 1.2% Ca^{2+}, and 1.1% K^+ are applied (Seinfeld and Pandis, 2006).

Inorganic particles can be solid and/or composed of an aqueous supersaturated solution. The assumption of aqueous aerosol for the acidity-sensitive semivolatile inorganic species (e.g., NH_3/NH_4^+ and HNO_3/NO_3^-) is found, though, to perform quite well with a series of aerosol LWC observations when the relative humidity is above 40% (Bougiatioti et al., 2016; Guo et al., 2015, 2017a). However, Cheng et al. (2022) recently indicated that although under high relative humidity conditions, both assumptions may perform almost identically, the aqueous aerosol setup might perform better under high temperatures (>10 ℃) and low relative humidity (<60%) conditions, while the solid aerosol setup might perform better for lower temperatures. For this, the metastable aerosol setup is here applied for temperatures higher than 10 ℃ and RH lower than 60% or higher than 83%. On the other hand, the stable aerosol setup is applied mostly at lower temperatures (<5 ℃). We note, however, that in our case, there were only minimal differences (less than 1% in the simulated SIA concentrations during the cold period) between simulations with only metastable (liquid) and variable aerosol state assumptions in thermodynamic calculations.

89 Even though this work is focused on the SIA fine aerosol fraction, nitrate aerosols are explicitly calculated for both the fine
90 and coarse modes (i.e., unlike SO_4^{2-} and NH_4^+). The rationale behind this is that nitrate is found to significantly contribute to
91 the coarse aerosol sizes (Koulouri et al., 2008), indicating that a bulk approach may lead to an overestimation of the HNO_3/NO_3^-
92 partitioning in the model, especially in areas with intense NVC contribution, such as from sea salt and dust aerosols, and from
93 anthropogenic combustion. For this practical application, kinetic limitations (Pringle et al., 2010) by mass transfer and transport
94 between the nitric acid in the gas phase and the particulate nitrate in $PM_{2.5}$ and PM_{10} are here considered, with ISORROPIA-
95 II then re-distributing the respective masses between the gas and the aerosol phases. We note, however, that the coarse nitrate
96 is not further taken into account in the thermodynamic calculations, assuming for simplicity that the gaseous HNO_3, able to
97 condense in the coarse aerosol mode, partitions directly into the particulate bulk phase.

2.1.3 Emissions

99 Anthropogenic emissions were originally provided by the Copernicus Atmosphere Monitoring Service (CAMS). CAMS
00 provides the annual emission rates of CO, NH3, NMVOCs, NOX, PM10, PM2.5, and SO2 from the road, air, rail transport,
01 maritime (local and international shipping), mobile machinery, fuel production, industrial (paper, cement, minerals, metals,
02 etc.), stationary combustion, agriculture, waste, solvent use, and public power sectors. As evident, forest fires or biogenic
03 sources are not included in this dataset. CAMS adopts the GNFR sector classification and provides gridded data at 0.1 x 0.05
04 degrees. This dataset is then spatially refined over the domain of interest with the spatial disaggregation approach and tool
05 documented in Ramacher et al. (2021). In particular, the regional anthropogenic dataset is combined with GNFR-dependent
06 high-resolution spatial proxies (based on data from the European Pollutant and Transfer Register; E-PRTR, Global Human
07 Settlement Population; GHS-POP, Corine Land Cover; CLC, and OpenStreetMap; OSM) towards the spatial disaggregation
08 in 1x1 km2 : i) area sources emitted 80 % in the model's layer 1 and 20 % in layer 2 for domestic heating, combustion in
09 manufacturing industry, agriculture and farming, and other mobile sources and machinery, except for shipping, where
10 emissions are equally distributed in the first 4 layers of the model; ii) point (industrial sources emitted at the height of each
11 stack); and iii) line emissions (road and railway emissions emitted at 0m). We note that the top heights of layers 1, 2, 3, and 4
12 are 17.5, 37.5, 62.5, and 87.5 m above the ground, respectively. Annual emissions are then converted into hourly emission
13 rates using monthly, weekly, and daily distributions based on average European factors, except for the yearly profiles for public
14 power, refineries, and road emissions, where CAMS-TEMPO factors are applied (Guevara et al., 2021). The respective maps
15 of the total annual emission fields are presented in Fig. S1.
16 Sea salt emissions are calculated for this work following the parameterizations from Gong (2003) and Vignati et al. (2010).
17 The flux of the number of sea-spray particles is expressed as a function of the particle radius at 80% humidity and the 10 m
18 horizontal wind speed, assuming number median dry radius values of 0.09 and 0.794 μm for fine and coarse sea-spray particles,
19 along with geometric standard deviations of 1.5 and 2.0, respectively (Vignati et al., 2010). To further address the temperature
20 effects on the sea spray source fluxes, polynomial expressions derived based on laboratory (chamber) experiments (Salter et

Deleted: Anthropogenic emissions were originally provided by the Copernicus Atmosphere Monitoring Service (CAMS) and then improved over the domain of interest with the spatial disaggregation approach and tool documented in (Ramacher et al., 2021). CAMS provides the annual emission rates of CO, NH_3, NMVOCs, NO_X, PM_{10}, $PM_{2.5}$, and SO_2 from the road, air, rail transport, navigation, mobile machinery, fuel production, industrial (paper, cement, minerals, metals, etc.), stationary combustion, agriculture, waste, solvent use, and public power sectors. The dataset adopts the GNFR sector classification and provides gridded data at 0.1 x 0.05 degrees. This dataset is then combined with GNFR-dependent high-resolution spatial proxies (based on data from E-PRTR, GHS-POP, CLC, and OSM) towards the spatial disaggregation in 1x1 km^2 (area sources), point (industrial), and line emissions (road and railway emissions).

al., 2015) have been implemented. The total annual sea salt emissions, as calculated on-line by the model, are presented in the supplement (Fig. S1e).

Potassium (K^+) emissions from anthropogenic wood-burning processes are further considered in our calculations, owing to their significance for the thermodynamic equilibrium distribution of nitrogen-containing semivolatile compounds. For this, we apply monthly factors to the $PM_{2.5}$ emissions from the domestic heating sector to derive the respective particle K^+ fluxes. The non-sea salt $K^+/PM_{2.5}$ concentration ratios are derived from filter-based $PM_{2.5}$ measurements in the center of Athens (Paraskevopoulou et al., 2014), specifically at the Thissio supersite (see Sect. 2.3). Assuming that in domestic wood combustion episodes K^+ is directly emitted as part of the $PM_{2.5}$, an average fraction of 3.52% w/w contribution is here applied to the respective $PM_{2.5}$ emissions for the winter months, as obtained by a positive matrix factorization (PMF) in central Athens (Thissio) from December 2013 to March 2016 (Theodosi et al., 2018). SO_4^{2-} primary sources from residential combustion are also accounted for in the model, owing to the significance of their ambient concentrations, accounting here for a fraction of 3.7% w/w (Zhang et al., 2023) of the $PM_{2.5}$ emitted during domestic wood combustion episodes. We note, however, that although Zhang et al. (2023) indicate that NO_3^- and NH_4^+ can also be emitted from domestic combustion processes, the respective emission factors are found to be 3–4 times lower compared to SO_4^{2-}, i.e., accounting for only up to 1% of the $PM_{2.5}$ emitted mass. For this reason, no primary emissions for NO_3^-, and NH_4^+ are accounted for in this study. The total annual K^+ emission field from anthropogenic wood-burning processes derived for this study is presented in Fig. S1f.

2.1.4 Boundary conditions

The CAMS European regional ensemble reanalysis data is used to create boundary conditions for O_3, NO, NO_2, CO, NH_3, $PM_{2.5}$, PM_{10}, PAN, SO_2, and NMVOC concentrations (chemically split to the species treated by the local model). Due to the chemical advancements of the current work (SIA treatment), the CAMS global atmospheric composition forecast supports the boundary conditions for H_2O_2, N_2O_5, HNO_3, methacrolein/methyl vinyl ketone, N_2O_5, HNO_3, and HNO_4, along with sea salt aerosols in the fine and coarse sizes (not available on the regional scale). Furthermore, since the CAMS European regional ensemble reanalysis data only provide SIA concentrations as lumped species, we also use the respective global atmospheric composition forecast to derive the individual species (i.e., SO_4^{2-}, NO_3^-, and NH_4^+) normalized to the regional ensemble models' SIA concentration data. The same assumption is applied for dust aerosols since dust concentrations are only provided as a part of the PM_{10} fraction in the regional reanalysis data. NO_3^- in the coarse mode is directly derived from the global forecast data (where available). The boundary conditions interface (BCONCAMS) developed at Helmholtz-Zentrum Hereon was utilized for the interpolation of the CAMS regional ensemble and global forecast product and the mapping of the chemical species to the urban air quality model. The interface performs bilinear interpolation in the horizontal and linear interpolation in the vertical and projects the pollutant concentrations to the city domain. We note that several utilities allow the preparation of input files or the conversion of these to the necessary CityChem input formats. More details on the utilities used to produce the EPISODE-CityChem input files can be found in Karl et al. (2019).

2.1.5 Meteorology

The CTM EPISODE-CityChem is offline coupled with the mesoscale numerical weather prediction system Weather Research and Forecasting (WRF). WRF is setup with Lambert-Conformal map projection, two-way nesting, Thompson graupel scheme for microphysics, Monin-Obukhov (Janjic Eta) scheme for surface-layer parameterization, Noah Land-Surface model, and Mellor-Yamada-Janjic (Eta) TKE scheme for boundary layer. The meteorological simulations are initialized by the synoptic-scale meteorological reanalysis ensemble means (ECMWF ERA5). For this work, WRF is applied with a telescoping nesting (3 domains), with the innermost domain covering the CTM area with a 1x1 km^2 spatial resolution. Hourly varying meteorological variables used as inputs in the EPISODE-CityChem include pressure, air temperature, temperature gradient, relative humidity, sensible and latent heat fluxes, total solar radiation, cloud fraction, and the cloud LWC.

2.2 In-situ measurements

In-situ aerosol chemical composition measurements conducted at 1) the Thissio Air Monitoring Supersite and 2) the Piraeus monitoring station, both operated by the National Observatory of Athens, are here used to evaluate the model's ability to simulate the main SIAs (SO_4^{2-}, NH_4^+, and NO_3^-) in the GAA, Greece. The Thissio Air Monitoring Supersite (37.9732° N, 23.7180° E, 105 m a.s.l.) is located on the premises of the National Observatory of Athens, in central Athens. The site is far from major traffic roads, in a moderately populated residential area, and thus is considered representative of urban background conditions in the center of the Athens basin (Grivas et al., 2019; Panopoulou et al., 2020), as it serves as a receptor of pollutants from different sources and with various degrees of processing. Online measurements took place throughout 2019 at Thissio, apart from the period when the instrumentation for online aerosol SIA measurements was moved to the Piraeus site. Measurements were conducted at a central location during two periods in winter (10 December 2018 - 16 January 2019) and summer (11 June 2019 - 9 July 2019). The instruments in Piraeus were located on the 1st floor (9m above ground) of the Athens Metro terminal station building (Urban Rail Transport S.A., Athens, Greece; 37.9479º N, 23.6429º E, 10 m a.s.l.). The site is influenced to an extent by traffic emissions, being at a distance of 70 m from the coastal avenue in the Piraeus port area (Stavroulas et al., 2021).

High-temporal resolution measurements of non-refractory submicron aerosol chemical composition at both sites were performed with a quadrupole Aerosol Chemical Speciation Monitor (ACSM; Aerodyne Research Inc.; Ng et al., 2011), operated at a 30-minute temporal resolution. The instrument provides concentrations of ammonium, sulfate, nitrate, chloride, and organic matter. Details on the limits of detection, sampling, and calibration of the instrument can be found in Stavroulas et al. (2019, 2021). QA/QC of ACSM measurements included the comparison of the daily-averaged online and offline measurements. The estimation of sea salt, non-sea salt potassium, and dust was performed using the methodology of Sciare et al. (2005). Although the evaluation of dust concentrations is out of the scope of this study, we note that the estimation of atmospheric dust levels using the calcium ion as a proxy (Sciare et al., 2005) may be largely uncertain due to major contributions from other sources. It should also be noted that since ion chromatography quantifies mostly the inorganic

9

components, it is expected that interferences may occur for sulfate and nitrate, especially during winter, when nitrites, organic nitrates, and sulfates are variably present (Guo et al., 2016).

3 Results and discussion

3.1 Model evaluation

3.1.1 Sulfate

Observations indicate that the hourly SO_4^{2-} concentrations present only a slightly increasing trend from winter to summer 2019 over Athens (Fig. 2a). During the warm season, however, the scarcity or absence of precipitation in the region, along with increased transport through the boundaries and mostly the higher oxidation potential, resulted in an overall increase in SO_4^{2-} concentrations in the model (W/ SIA), although still lower compared to observations. The enhanced summer concentrations in the model are nonetheless in accordance with previous observational and modeling studies in the area (Athanasopoulou et al., 2015; Grivas et al., 2018; Paraskevopoulou et al., 2015; Theodosi et al., 2018), suggesting that the majority of SO_4^{2-} mainly originates from long-range transport (e.g., Balkan countries and the wider Black Sea region) due to fossil fuel combustion in power production and other industrial plants (Aksoyoglu et al., 2017). This is also clearly shown by the present sensitivity model calculations, indicating that when the local SO_4^{2-} production via aqueous-phase SO_2 oxidation is neglected (W/O SIA), the simulated SO_4^{2-} concentrations remain practically unchanged in most of the cases, especially during the warm periods. EPISODE-CityChem captures the observed hourly SO_4^{2-} surface levels in Piraeus and Thissio, with a correlation coefficient (r) of 0.46 and an annual mean bias of -1.2 µg m^{-3} (Fig. 2a), partly attributed to the temporal variation of emissions, which is largely based on Europe-wide factors provided along with the CAMS-REG yearly data. The model tends to overall underestimate the observations, presenting for 2019 a negative normalized mean bias (nMB) of -42%. Our simulations nevertheless indicate that the underestimation of the modeled SO_4^{2-} concentrations should be mainly due to the too low long-range transport in the area through the boundaries, since only a weak local SO_4^{2-} formation is supported by the model. Indeed, when comparing the base simulation (W/ SIA) with the W/O SIA sensitivity simulation, where the local SO_4^{2-} production in cloud droplets is neglected, only a slight increase in the surface SO_4^{2-} concentrations is illustrated, without any noteworthy change (< 1%) in the respective correlation statistics. On the other hand, the underrepresentation of SO_x (= SO_2 + SO_4^{2-}) local emissions, or even a too slow SO_2 oxidation in the gas phase, could further contribute to the model's underestimation of the observed values. Last, although WRF accurately predicts temperature and humidity fields, it tends to overestimate wind speed (see Table S1 in the Supplement). This has the effect of enhanced ventilation and dispersion of SO_4^{2-} (and the rest of SIAs), which may partially explain the observed negative biases in the simulated pollutants under study.

10

Deleted: .

3.1.2 Nitrate

The observed and modeled NO_3^- concentrations increase during the cold period (Fig. 2b), presenting a pronounced seasonality. The increase mentioned above is caused by both the formation of NH_4NO_3 under low ambient temperatures (Theodosi et al., 2018) and the presence of non-volatile potassium cations from domestic heating processes, which can significantly promote the formation of KNO_3. On the contrary, the observed NO_3^- concentrations are considerably reduced in summer (Liakakou et al., 2022; Paraskevopoulou et al., 2015), owing to the thermal instability and volatilization of the NH_4NO_3.

Sensitivity model simulations clearly indicate that NO_3^- is a local pollutant rather than a transported one in the GAA. This agrees with previous modeling studies where road traffic is found to significantly contribute to NO_3^- in eastern Europe (Aksoyoglu et al., 2017). Indeed, when the thermodynamics are neglected in model calculations (W/O SIA), NO_3^- concentrations are severely underestimated over GAA in almost all seasons of the year, except for some cases during the summer months (July and, to a lesser extent, August). Although EPISODE-CityChem tends to calculate very low NO_3^- levels during the warm period for the base simulation (W/ SIA), the maxima during July and August due to the contribution of long-range transport from biomass burning processes (such as wildfires in Attica and the island of Evia in July and August 2019) seem not to be well captured by the model. On the other hand, the W/O Kbb sensitivity model simulation clearly indicates that the presence of K^+ associated with domestic heating processes plays a crucial role in NO_3^- formation during the winter period, leading overall to a lower nMB compared to the base simulation (i.e., -63% vs. -61%). This, yet, is in accordance with previous findings in the region, where a good correlation between K^+ with OC, EC, and NO_3^- has been observed during winter (Fourtziou et al., 2017; Theodosi et al., 2018), thus clearly supporting their common origin during the cold period. In more detail, residential biomass burning processes are found to be directly responsible for the winter maxima measured over GAA, while intense Saharan dust episodes under the local southerly winds may also have an impact on the spring peak.

A better correlation compared to that of SO_4^{2-} is found when comparing the model and the measurements for the hourly NO_3^- surface levels (r = 0.58). The model, however, tends to overall underestimate the observations, with a slightly negative bias of around -0.4 μg m^{-3} and an nMB of roughly -61% for the year 2019, mainly due to the too low summertime simulated concentrations (Fig. 2b). We note, nevertheless, that an underestimation of the observed concentrations is here expected since, on the one hand, some ammonia sources, such as from agricultural soils, are currently omitted in the model, and on the other hand, species that may be accounted for in the observational data, such as nitrites and organic nitrates that may also be present during winter and partition in the particulate phase (Guo et al., 2016), are not yet included in the presented chemical mechanism. Still, correlation statistics clearly denote that the local HNO_3 partitioning in the particulate phase is the main pathway of fine particulate NO_3^- formation in the study area, and more specifically, that the presence of K^+, either from domestic burning processes or dust events, plays a crucial role in the NO_3^- concentration distributions.

11

3.1.3 Ammonium

The observed NH_4^+ concentrations (Fig. 2c) generally present a similar seasonal pattern to that of SO_4^{2-}, although somehow with a more intense trend during the warm season. As already found in previous works (Mantas et al., 2014; Paraskevopoulou et al., 2015; Theodosi et al., 2018), observations of NH_4^+ and SO_4^{2-} are highly correlated (r = 0.79) indicating that nss-SO_4^{2-} can be considered at least partially neutralized by NH_4^+. The simulated sulfate/ammonium ratio for the base simulation (r = 0.73) shows that sulfate exists mainly in the model in the form of NH_4HSO_4 and $(NH_4)_2SO_4$ in the two sites (i.e., Thissio and Piraeus), in agreement with previous studies in the wider eastern Mediterranean area (Athanasopoulou et al., 2008; Bardouki et al., 2003; Fourtziou et al., 2017; Koulouri et al., 2008). Nevertheless, during the cold season, NH_4^+ is also found to be significantly correlated with NO_3^- (r = 0.62), indicative of NH_4NO_3 formation, respectively. Note, however, that for this work, the non-sea salt chloride is not considered in model calculations, so the nss-NH_4Cl does not contribute to the calculated NH_4 concentrations.

The base case simulation of EPISODE-CityChem captures the observed NH_4^+ hourly surface observations in Piraeus and Thissio with a correlation coefficient (r) of 0.57 and a negative mean bias of -0.4 μg m^{-3} (Fig. 2f), with a calculated negative nMB of -46% for 2019. However, when the thermodynamic calculations are neglected in the model in the W/O SIA simulation (i.e., accounting only for the transport from the model's boundaries contributing to the NH_4^+ levels), the agreement tends to improve, leading to a correlation coefficient (r) of 0.61, a negative mean bias of -0.2 μg m^{-3}, and a negative nMB of -22% (Fig. 2f). This can be explained due to the volatilization of NH_4^+ for the base simulation when thermodynamics are taken into account in the model, which overall shifts NH_4^+ to gas-phase NH_3 (Guo et al., 2018).

The significance of aerosol pH levels on NH_4^+ volatilization is further supported by the model sensitivity simulation when the contribution of K^+ from domestic heating processes is neglected in the thermodynamic calculations (W/O Kbb). Indeed, the absence of K^+ increases the acidity in the aerosol phase and thus enhances the gas/particle partitioning of NH_3/NH_4^+. Overall, the improved correlation of model results with observations in the absence of K^+ from domestic heating compared to the base case simulation (i.e., r = 0.61, bias = -0.3, and nMB = -37%) indicates that the model misses primary NH_3 emissions from sources like road transport, that could contribute up to 10% to NH_4^+ ambient levels (Aksoyoglu et al., 2017), or from non-urban sources, such as the volatilization of animal waste and synthetic fertilizers, biomass combustion, and losses from natural soils (e.g., Fameli and Assimakopoulos, 2016)

3.2 Spatial model concentration fields

The mapping of the main SIAs at ground level, as simulated by EPISODE-CityChem averaged for the winter (January, February, and December 2019) and summer (June, July, and August 2019) periods, is presented in Fig. 3. Additionally, the spatio-temporal totals of the SIA-related tracer emissions are presented in Fig. S2. During both seasons, high SO_4^{2-} levels are simulated near the major emission hotspots, such as shipping routes around the Ports of Piraeus and Eleusis and large combustion plants in the Thriassion Plain (Fig. 1), where the vast majority of the surface SO_2 emissions in the GAA occur.

During summer (Fig. 3b), the predicted SO_4^{2-} surface concentrations are close to 2.86 ± 0.92 µg m^{-3} in the center of Athens and the suburbs, while during winter (Fig. 3a) the season mean simulated concentrations vary between 1.31 and 4.45 µg m^{-3}. The results indicate that long-range transport is an important contributor to SO_4^{2-} surface concentrations in the area, which are maximized during the summer due to enhanced photochemical activity. On average, SO_4^{2-} is calculated to have an annual mean surface concentration of 2.15 ± 0.88 µg m^{-3} for the year 2019 in the model domain. Sensitivity model calculations confirmed this, showing that chemical production in the model domain can support up to 10% of the wintertime SO_4^{2-} surface concentrations (Fig. 4a), mainly in higher altitude areas, such as Parnitha Mt. (Fig. 1), where cloudiness is enhanced and the increased cloud LWC promotes the aqueous phase oxidation of ambient SO_2. Around the city center, however, the chemical formation contribution to the surface SO_4^{2-} levels is calculated to be rather low (roughly 4%).

The average fine NO_3^- concentrations in the model are calculated to vary between 0.05 and 1.50 µg m^{-3} during the cold period (Fig. 3c). A mean NO_3^- concentration of 0.51 ± 0.20 µg m^{-3} is simulated during the winter months, while only 0.05 ± 0.05 µg m^{-3} is calculated during the summer (Fig. 3d). In the model domain, NO_3^- registered an annual mean surface concentration of 0.24 ± 0.23 µg m^{-3} for 2019. In contrast, however, to the SO_4^{2-} surface concentrations, NO_3^- levels present notable spatial variability, with much higher concentrations calculated near rather than away from the city center during the winter, compared to the negligible concentrations in the warm season. This indicates that NO_3^- formation significantly depends on the local meteorological conditions (i.e., temperature and relative humidity) along with the anthropogenic emissions of precursor species that are widespread in the GAA (Fig. 1), mainly from traffic, and especially the presence of NVCs such as K+ from domestic heating in winter that can support an increase in NO_3^- surface concentrations of about $10 \pm 4\%$ in the model domain (Fig. 4d). It is noted that in this study, NO_3^- is only either formed in the model domain as a secondary product or transported from the boundaries, without any primary contribution. However, the enhanced concentrations around the city center in the model clearly indicate that NO_3^- is mainly a local pollutant rather than a transported one over the GAA. The latter is further supported through sensitivity model calculations performed for this work, demonstrating that when thermodynamics are accounted for in the model (Fig. 4c), more than 80% of the NO_3^- surface concentrations on an annual basis in downtown Athens (Fig. 1) are directly attributed to the HNO_3 gas/particle partitioning.

The average surface NH_4^+ concentrations in the model are calculated to be without strong annual variability in the GAA for 2019. For the cold period (Fig. 3e), the model simulates that NH_4^+ concentration varies between 0.30 in the suburbs and 1.40 µg m^{-3} around the city center, while for the summertime it is between 0.33 and 1.18 µg m^{-3}, respectively (Fig. 3f). For the year 2019, NH_4^+ is calculated to have an annual mean surface concentration of 0.58 ± 0.14 µg m^{-3} in the model domain. Model simulations show that the available anthropogenic NH_3 emissions in the model domain tend to quickly neutralize the primary strong acids present in the urban atmosphere of Athens, like H_2SO_4 and HNO_3, which subsequently partition into the aerosol aqueous phase in the form of the ammonium ion. As already discussed in Sect. 3.1.3, when thermodynamics are included in model simulation, an increase in volatilization of NH_4^+ is calculated that, on an annual basis, can support a decrease in its concentrations up to 70% in the suburbs (Fig. 4e). On the other hand, much lower NH_4^+ volatilization is calculated around the Thriassion Plain, where combustion plants exist, as well as in the region's major port zones (Fig. 1), due to primary NH_3

13

30 sources. The latter indicates that although traffic, solid and water waste management facilities, and certain industrial processes

31 (e.g., refineries, cement manufacturing, livestock production) seem to be the main NH_3 sources in urban areas (Liakakou et al.,

32 2023), ammonia may also be strongly related to agricultural activities and soil sources in rural areas, which in turn significantly

33 impacts NH_4^+ concentrations; however, NH_3 emissions from such sectors are not currently included in our model. Additionally,

34 emissions from domestic heating may also have some impact on NH_3 surface levels (Fig. 4f), since in the presence of non-

35 volatile potassium cation such as from biomass burning processes, the formation of KNO_3 is promoted and thus the gas/particle

36 partitioning of NH_3 is reduced (12 ± 2 %).

3.3 Atmospheric water and acidity

38 Particle LWC and aerosol pH are important parameters of the aerosol phase; however, limited in situ observations of aerosol

39 pH exist due to the non-conserved nature of H^+ and the dissociation of inorganic and organic electrolytes in the particulate

40 phase. Since ion balance proxy methods generally lead to miscalculations of aerosol acidity levels, thermodynamic model

41 calculations can be considered a reliable tool for such calculations (Hennigan et al., 2015). The acidity levels in an urban

42 environment are primarily governed by the atmospheric LWC and the aqueous-phase proton concentration ($[H^+]$). The impacts

43 of cloud LWC and aerosol water on atmospheric acidity significantly differ; cloud liquid water is primarily determined by

44 meteorological conditions, while aerosol water is subject to chemical equilibrium with atmospheric water vapors. Thus, the

45 hygroscopicity of the dissolved aerosol species plays a significant role in governing the aerosol water content under specific

46 relative humidity levels (Pye et al., 2020). Moreover, the pH levels in clouds are found to be notably higher (up to four units;

47 Seinfeld and Pandis, 2006) in comparison to aerosols, owing to the dilute conditions prevailing in them. On the contrary,

48 aerosol acidity is determined not only by the equilibrium between acidic and alkaline species but also by the relative

49 concentrations of such species that partition in the particulate phase under favorable temperature and relative humidity

50 conditions (Pye et al., 2020).

51 Figure 5 illustrates the averaged pH levels of fine aerosols and the respective particulate water content on the surface for winter

52 and summer, as calculated by EPISODE-CityChem. The calculated pH for fine aerosols over the GAA can be rather acidic,

53 with an average value of 4.81 ± 0.93 during winter (Fig. 5a) and 2.20 ± 1.00 during summer (Fig. 5b), varying spatially between

54 2.38 - 7.58 and 0.79 - 5.82, respectively. Minimum pH values are calculated to differ by roughly one unit, indicating an overall

55 10-fold increase in the aerosol H^+/LWC ratio from summer to winter periods in the model. Such a variation in the aerosol

56 acidity can be directly attributed to the significantly different meteorological parameters between the two seasons, illustrating

57 the importance of the increased relative humidity levels on aerosol pH values during the cold period. Nonetheless, the

58 persistence of strong acidity in fine aerosols can also be attributed to the thermodynamic equilibrium between NH_4^+ and NH_3

59 that overall promotes the NH_x (= $NH_3 + NH_4^+$) volatilization in the model. This is in accordance with other studies where,

60 although gaseous NH_3 may be abundant, the pH values of $PM_{2.5}$ remain acidic (Ding et al., 2019). Note, however, that for this

61 study we only account for the water associated with the inorganic aerosol component; thus, the model may slightly

62 underestimate the particulate water by 0.15-0.23 units compared to the pH predicted with total water (Guo et al., 2015). This

14

63 value is likely an upper bound on the error since organic aerosol mass fractions in the specific location were high (~60%; Guo

64 et al., 2015; Stavroulas et al., 2019). On the other hand, the significantly higher maximum pH values during wintertime cannot

65 be only attributed to meteorology. In accordance with previous studies, higher aerosol pH levels can be directly associated

66 with the presence of NVCs emanating from wood-burning processes (Bougiatioti et al., 2016; Zhang et al., 2015). For

67 completeness, the calculated surface aerosol water concentrations for winter (Fig. 5c) and summer (Fig. 5d) are also provided.

68 The long-range transport of SIA along with the emissions of its precursors, such as SO_2 and NO_X, tend to also decrease local

69 cloud pH levels in the model. It should be mentioned that EPISODE-CityChem does not calculate, but instead only reads the

70 cloud LWC and the cloud cover from meteorological files in the region, meaning that no transport of clouds exists in the model

71 domain. During the winter season (Fig. 5e), higher cloud pH values have been generally calculated as compared to the summer

72 season (not shown). The cloud pH is calculated to vary between 3.50 and 6.70 during the wintertime over Athens, mostly in

73 the suburbs where the higher cloudiness exists, owing to the orography of the regions. On the contrary, during the summer,

74 the model calculates clouds of higher acidity (i.e., up to ~0.28 pH units). This, however, can be attributed mainly to the relative

75 absence of cloud water during the warm period in the model, along with the increased transport of acidic compounds like

76 sulfates (i.e., very concentrated solutions lead to strongly acidic pH values). Note, however, that the potential impact of mineral

77 dust, particularly calcium, on cloud H^+ concentrations has been neglected in the above calculations. Such an assumption could

78 potentially lead to an overestimation of cloud acidity, especially during the dust event periods (mainly late winter and spring).

79 A further constraint in the assessment of cloud acidity pertains to the exclusion of low-molecular-weight organic acids (e.g.,

80 formic and acetic acids), which may also result in some degree of miscalculation of the cloud acidity levels.

81 **4 Summary and conclusions**

82 For this work, the ISORROPIA II thermodynamic model has been coupled to the urban-scale EPISODE-CityChem CTM to

83 calculate the gas/particle partitioning of NH_3/NH_4^+ and HNO_3/NO_3^-, providing insights into complex interactions in a major

84 Eastern Mediterranean urban agglomeration. While the model tends to generally underestimate the SIA measurements over

85 the Greater Area of Athens, it tracks their observed daily variation at Piraeus and Thissio monitoring stations. SIA formation

86 appears to significantly depend on the ambient precursor gasses (SO_2, NO_X, and NH_3), which represent an important fraction

87 (i.e., up to 20% during both cold and warm periods) of $PM_{2.5}$ in the model domain, especially in suburban areas. Nevertheless,

88 long-range transport is found to be a critical factor in determining the SIA ambient concentrations, especially for SO_4^{2-}. Indeed,

89 the model's underestimation of observed SO_4^2 concentrations rather indicates a too weak transport from the boundaries than a

90 too low secondary formation from primary SO_x sources. Respectively, the lower NH_4^+ concentrations compared to the observed

91 values generally follow the variations of the simulated SO_4^{2-}, as also denoted by the derived sulfate/ammonium ratio, where

92 sulfate is mainly in the form of NH_4HSO_4 and $(NH_4)_2SO_4$. Specifically, during the cold period, the relatively basic aerosol pH

93 values enhance the volatilization of NH_4^+ in the model, and along with possibly missing NH_3 sources, the model tends to

94 underestimate the measurements.

The inclusion of non-volatile cations originated from biomass burning sources, along with sea salt and dust aerosols, has nevertheless had a critical impact on the ion balance and thus the partitioning of semi-volatile compounds (i.e., nitrate and ammonium) in the model. Although this study is focused on the fine PM fraction, we note that high nitrate concentrations have been found to be well correlated with increased concentrations of super-micron dust and sea spray particles (Allen et al., 2015), indicating the importance of crustal species in the HNO_3/NO_3^- partitioning. Still, besides the presence of sea salt and dust aerosols, the inclusion of K^+ from domestic wood-burning combustion sources in the aerosol thermodynamic calculations is found to affect the ion balance and thus the formation of NO_3^-, due to a more effective partitioning in the aerosol phase during the cold and humid conditions. NO_3^- concentrations for 2019 exhibit a relatively lower value in comparison to the observations, with a correlation coefficient of 0.58 and a normalized mean bias of -61%. However, the model performs better in simulating NO_3^- concentrations as compared to SO_4^{2-} (i.e., r = 0.46) and NH_4^+ (i.e., r = 0.57), suggesting a satisfactory representation of the HNO_3/NO_3^- partitioning. On the other hand, the volatilization of NH_4^+ due to a decrease in aerosol pH (especially during the warm period) tends to shift NH_4^+ to the gas-phase, further indicating missing NH_3 sources in the model.

It is well established that SIAs play an important role in urban air quality and can have detrimental effects on the environment and human health. Thus, reducing emissions of their precursors via measures including, inter alia, the extensive use of sustainable energy, mobility, and agriculture is crucial for mitigating such effects in the long term. The continuation of such policies on the European level appears critical, especially in view of new air quality management legislation in the EU that will set very ambitious PM standards for the protection of public health, which will be difficult to attain unless sweeping emission cutbacks are implemented. Moreover, despite the fact that the reduction in primary pollutants like SO_2 and NO_X can also reduce the acidity of cloud water and precipitation (Watmough et al., 2016), fine aerosols may still remain highly acidic in a future atmosphere due to the respective NH_3 volatilization in the particulate phase (Baker et al., 2021; Lawal et al., 2018). On the other hand, it is shown here that, accounting for the K^+ sources from domestic wood burning in the model, significantly higher aerosol pH values can be locally supported during the winter compared to the warm period, where K^+ is mostly associated with Saharan dust outbreaks in the GAA (Theodosi et al., 2018). Nevertheless, such a discrepancy in the response of the fine aerosol pH to emission controls also has noteworthy implications for the toxicity of atmospheric particles, especially during the cold period where domestic wood burning may consist of an additional source of harmful air pollution. Such complex chemical interactions have not yet, however, been comprehensively acknowledged in urban-scale studies (Zhang et al., 2022).

In this study, the high spatiotemporal resolution of EPISODE-CityChem (up to 100 x 100 m^2, 1 h) with the improved representation of the inorganic aerosols delivers a beyond-the-state-of-the-art characterization of the fine particulate load over the GAA. Focusing further on air-quality studies in polluted urban domains, several initiatives are underway aimed at improving EPISODE-CityChem's modeling of aerosols and the respective chemical processes. These include coupling with aerosol microphysical schemes that will account for new particle formation and aerosol aging through coalescence and condensation (e.g., Karl et al., 2023). Such developments aim to improve the model's ability to represent the composition and size distribution of fine PM. A better characterization of aerosol chemical speciation, like the consideration of organic aerosols,

16

is expected to also improve the aerosol hygroscopicity calculations in the model, especially within the boundary layer where the contribution of water-soluble organics to total aerosol mass is important (i.e., Bougiatioti et al., 2016). The KPP software for solving stiff numerical systems has already been coupled to the model to integrate the gas phase photochemistry schemes, and based on this development, more explicit chemical schemes are planned to be available in the model. Furthermore, gas-phase organic species can also be oxidized in the interstitial cloud space and form water-soluble compounds like aldehydes, which rapidly partition into droplets. In the presence of oxidants (e.g., OH and NO_3 radicals), the dissolved organics can also undergo chemical conversions and form low-volatile organics that remain partially in the aerosol phase. A state-of-the-art multiphase chemical scheme (e.g., Myriokefalitakis et al., 2022) is therefore planned to be coupled to the model to account for such an aerosol formation process in an urban area. Additionally, parameterizations of marine dimethylsulfide (DMS) and organic aerosol primary sources in the model are currently under consideration.

The proposed model framework, coupled with emission reduction scenarios, may enable a thorough investigation of the regulations and interventions that can efficiently curtail air pollution in the GAA and, consequently, its health impacts, providing a valuable decision support tool to the air quality management authorities in view of the realignment with the new air quality standards that will be inevitable in the near future, given the present state of air quality in Greece. Anticipated advancements in model parallelization and code architecture are expected to facilitate computationally efficient urban simulations and the creation of state-of-the-art forecasting systems capable of generating high-resolution air quality predictions for multiple urban regions in Europe up to street level. Overall, providing such an urban-scale modeling tool allows for a more accurate articulation of strategies for air quality management, including the optimization of monitoring protocols as well as the mitigation of emissions from various activity sectors and adverse effects.

5 References

Aksoyoglu, S., Ciarelli, G., El-Haddad, I., Baltensperger, U., and Prévôt, A. S. H.: Secondary inorganic aerosols in Europe: sources and the significant influence of biogenic VOC emissions, especially on ammonium nitrate, Atmospheric Chemistry and Physics, 17, 7757–7773, https://doi.org/10.5194/acp-17-7757-2017, 2017.

Alexander, B., Park, R. J., Jacob, D. J., and Gong, S.: Transition metal-catalyzed oxidation of atmospheric sulfur: Global implications for the sulfur budget, Journal of Geophysical Research, 114, D02309, https://doi.org/10.1029/2008JD010486, 2009.

Allen, H. M., Draper, D. C., Ayres, B. R., Ault, A., Bondy, A., Takahama, S., Modini, R. L., Baumann, K., Edgerton, E., Knote, C., Laskin, A., Wang, B., and Fry, J. L.: Influence of crustal dust and sea spray supermicron particle concentrations and acidity on inorganic NO&lt;sub&gt;3&lt;/sub&gt;&lt;sup&gt;&amp;minus;&lt;/sup&gt; aerosol during the 2013 Southern Oxidant and Aerosol Study, Atmospheric Chemistry and Physics, 15, 10669–10685, https://doi.org/10.5194/acp-15-10669-2015, 2015.

Athanasopoulou, E., Tombrou, M., Pandis, S. N., and Russell, A. G.: The role of sea-salt emissions and heterogeneous chemistry in the air quality of polluted coastal areas, Atmospheric Chemistry and Physics, 8, 5755–5769, https://doi.org/10.5194/acp-8-5755-2008, 2008.

Athanasopoulou, E., Vogel, H., Vogel, B., Tsimpidi, A. P., Pandis, S. N., Knote, C., and Fountoukis, C.: Modeling the meteorological and chemical effects of secondary organic aerosols during an EUCAARI campaign, Atmospheric Chemistry and Physics, 13, 625–645, https://doi.org/10.5194/acp-13-625-2013, 2013.

Athanasopoulou, E., Protonotariou, A. P., Bossioli, E., Dandou, A., Tombrou, M., Allan, J. D., Coe, H., Mihalopoulos, N., Kalogiros, J., Bacak, A., Sciare, J., and Biskos, G.: Aerosol chemistry above an extended archipelago of the eastern Mediterranean basin during strong northern winds, Atmospheric Chemistry and Physics, 15, 8401–8421, https://doi.org/10.5194/acp-15-8401-2015, 2015.

Athanasopoulou, E., Protonotariou, A., Papangelis, G., Tombrou, M., Mihalopoulos, N., and Gerasopoulos, E.: Long-range transport of Saharan dust and chemical transformations over the Eastern Mediterranean, Atmospheric Environment, 140, 592–604, https://doi.org/10.1016/j.atmosenv.2016.06.041, 2016.

Atkinson, R., Baulch, D. L., Cox, R. A., Crowley, J. N., Hampson, R. F., Hynes, R. G., Jenkin, M. E., Rossi, M. J., and Troe, J.: Evaluated kinetic and photochemical data for atmospheric chemistry: Volume I - gas phase reactions of Ox, HOx, NOx and SOx species, Atmospheric Chemistry and Physics, 4, 1461–1738, https://doi.org/10.5194/acp-4-1461-2004, 2004.

Baker, A. R., Kanakidou, M., Nenes, A., Myriokefalitakis, S., Croot, P. L., Duce, R. A., Gao, Y., Guieu, C., Ito, A., Jickells, T. D., Mahowald, N. M., Middag, R., Perron, M. M. G., Sarin, M. M., Shelley, R., and Turner, D. R.: Changing atmospheric acidity as a modulator of nutrient deposition and ocean biogeochemistry, Science Advances, 7, eabd8800, https://doi.org/10.1126/sciadv.abd8800, 2021.

Bardouki, H., Liakakou, H., Economou, C., Sciare, J., Smolík, J., Ždímal, V., Eleftheriadis, K., Lazaridis, M., Dye, C., and Mihalopoulos, N.: Chemical composition of size-resolved atmospheric aerosols in the eastern Mediterranean during summer and winter, Atmospheric Environment, 37, 195–208, https://doi.org/10.1016/S1352-2310(02)00859-2, 2003.

Basagaña, X., Jacquemin, B., Karanasiou, A., Ostro, B., Querol, X., Agis, D., Alessandrini, E., Alguacil, J., Artiñano, B., Catrambone, M., De La Rosa, J. D., Díaz, J., Faustini, A., Ferrari, S., Forastiere, F., Katsouyanni, K., Linares, C., Perrino, C., Ranzi, A., Ricciardelli, I., Samoli, E., Zauli-Sajani, S., Sunyer, J., and Stafoggia, M.: Short-term effects of particulate matter constituents on daily hospitalizations and mortality in five South-European cities: Results from the MED-PARTICLES project, Environment International, 75, 151–158, https://doi.org/10.1016/j.envint.2014.11.011, 2015.

Basla, B., Agresti, V., Balzarini, A., Giani, P., Pirovano, G., Gilardoni, S., Paglione, M., Colombi, C., Belis, C. A., Poluzzi, V., Scotto, F., and Lonati, G.: Simulations of Organic Aerosol with CAMx over the Po Valley during the Summer Season, Atmosphere, 13, 1996, https://doi.org/10.3390/atmos13121996, 2022.

Bougiatioti, A., Nikolaou, P., Stavroulas, I., Kouvarakis, G., Weber, R., Nenes, A., Kanakidou, M., and Mihalopoulos, N.: Particle water and pH in the eastern Mediterranean: source variability and implications for nutrient availability, Atmospheric Chemistry and Physics, 16, 4579–4591, https://doi.org/10.5194/acp-16-4579-2016, 2016.

Brandt, F., Bosbach, D., Krawczyk-Barsch, E., Arnold, T., and Bernhard, G.: Chlorite dissolution in the acid ph-range: a

18

combined microscopic and macroscopic approach, Geochimica et Cosmochimica Acta, 67, 1451–1461, https://doi.org/10.1016/S0016-7037(02)01293-0, 2003.

Cheng, B., Wang-Li, L., Classen, J., and Bloomfield, P.: Performance of a Thermodynamic Model for Predicting Inorganic Aerosols in the Southeastern U.S., Atmosphere, 13, 1977, https://doi.org/10.3390/atmos13121977, 2022.

Clegg, S. L., Brimblecombe, P., and Wexler, A. S.: Thermodynamic Model of the System H+–NH4+–SO42––NO3––H2O at Tropospheric Temperatures, J. Phys. Chem. A, 102, 2137–2154, https://doi.org/10.1021/jp973042r, 1998.

Damian, V., Sandu, A., Damian, M., Potra, F., and Carmichael, G. R.: The kinetic preprocessor KPP-a software environment for solving chemical kinetics, Computers & Chemical Engineering, 26, 1567–1579, https://doi.org/10.1016/S0098-1354(02)00128-X, 2002.

Denby, B. R., Gauss, M., Wind, P., Mu, Q., Grøtting Wærsted, E., Fagerli, H., Valdebenito, A., and Klein, H.: Description of the uEMEP_v5 downscaling approach for the EMEP MSC-W chemistry transport model, Geoscientific Model Development, 13, 6303–6323, https://doi.org/10.5194/gmd-13-6303-2020, 2020.

Dimitriou, K., Grivas, G., Liakakou, E., Gerasopoulos, E., and Mihalopoulos, N.: Assessing the contribution of regional sources to urban air pollution by applying 3D-PSCF modeling, Atmospheric Research, 248, 105187, https://doi.org/10.1016/j.atmosres.2020.105187, 2021.

Ding, J., Zhao, P., Su, J., Dong, Q., Du, X., and Zhang, Y.: Aerosol pH and its driving factors in Beijing, 19, 7939–7954, https://doi.org/10.5194/acp-19-7939-2019, 2019.

Driscoll, C. T., Driscoll, K. M., Mitchell, M. J., and Raynal, D. J.: Effects of acidic deposition on forest and aquatic ecosystems in New York State, Environ Pollut, 123, 327–336, https://doi.org/10.1016/s0269-7491(03)00019-8, 2003.

Driscoll, C. T., Driscoll, K. M., Fakhraei, H., and Civerolo, K.: Long-term temporal trends and spatial patterns in the acid-base chemistry of lakes in the Adirondack region of New York in response to decreases in acidic deposition, Atmospheric Environment, 146, 5–14, https://doi.org/10.1016/j.atmosenv.2016.08.034, 2016.

Fameli, K.-M. and Assimakopoulos, V. D.: The new open Flexible Emission Inventory for Greece and the Greater Athens Area (FEI-GREGAA): Account of pollutant sources and their importance from 2006 to 2012, Atmospheric Environment, 137, 17–37, https://doi.org/10.1016/j.atmosenv.2016.04.004, 2016.

Fountoukis, C. and Nenes, A.: ISORROPIA II: a computationally efficient thermodynamic equilibrium model for K+ – Ca 2+ –Mg 2+ –NH4+ –Na+ –SO4 2- –NO3-, Atmospheric Chemistry and Physics, 7, 4639–4659, https://doi.org/10.5194/acp-7-4639-2007, 2007.

Fountoukis, C., Racherla, P. N., Denier van der Gon, H. a. C., Polymeneas, P., Charalampidis, P. E., Pilinis, C., Wiedensohler, A., Dall'Osto, M., O'Dowd, C., and Pandis, S. N.: Evaluation of a three-dimensional chemical transport model (PMCAMx) in the European domain during the EUCAARI May 2008 campaign, Atmospheric Chemistry and Physics, 11, 10331–10347, https://doi.org/10.5194/acp-11-10331-2011, 2011.

Fourtziou, L., Liakakou, E., Stavroulas, I., Theodosi, C., Zarmpas, P., Psiloglou, B., Sciare, J., Maggos, T., Bairachtari, K., Bougiatioti, A., Gerasopoulos, E., Sarda-Estève, R., Bonnaire, N., and Mihalopoulos, N.: Multi-tracer approach to characterize domestic wood burning in Athens (Greece) during wintertime, Atmospheric Environment, 148, 89–101, https://doi.org/10.1016/j.atmosenv.2016.10.011, 2017.

Franklin, M., Koutrakis, P., and Schwartz, J.: The Role of Particle Composition on the Association Between PM2.5 and Mortality, Epidemiology, 19, 680–689, https://doi.org/10.1097/EDE.0b013e3181812bb7, 2008.

Gong, S. L.: A parameterization of sea-salt aerosol source function for sub- and super-micron particles, Global Biogeochemical Cycles, 17, https://doi.org/10.1029/2003GB002079, 2003.

Gratsea, M., Athanasopoulou, E., Kakouri, A., Richter, A., Seyler, A., and Gerasopoulos, E.: Five Years of Spatially Resolved Ground-Based MAX-DOAS Measurements of Nitrogen Dioxide in the Urban Area of Athens: Synergies with In Situ Measurements and Model Simulations, Atmosphere, 12, 1634, https://doi.org/10.3390/atmos12121634, 2021.

Grivas, G., Cheristanidis, S., Chaloulakou, A., Koutrakis, P., and Mihalopoulos, N.: Elemental Composition and Source Apportionment of Fine and Coarse Particles at Traffic and Urban Background Locations in Athens, Greece, Aerosol Air Qual. Res., 18, 1642–1659, https://doi.org/10.4209/aaqr.2017.12.0567, 2018.

Grivas, G., Stavroulas, I., Liakakou, E., Kaskaoutis, D. G., Bougiatioti, A., Paraskevopoulou, D., Gerasopoulos, E., and Mihalopoulos, N.: Measuring the spatial variability of black carbon in Athens during wintertime, Air Qual Atmos Health, 12, 1405–1417, https://doi.org/10.1007/s11869-019-00756-y, 2019.

19

Grivas, G., Athanasopoulou, E., Kakouri, A., Bailey, J., Liakakou, E., Stavroulas, I., Kalkavouras, P., Bougiatioti, A., Kaskaoutis, D. G., Ramonet, M., Mihalopoulos, N., and Gerasopoulos, E.: Integrating in situ Measurements and City Scale Modelling to Assess the COVID–19 Lockdown Effects on Emissions and Air Quality in Athens, Greece, Atmosphere, 11, 1174, https://doi.org/10.3390/atmos11111174, 2020.

Guevara, M., Jorba, O., Tena, C., Denier Van Der Gon, H., Kuenen, J., Elguindi, N., Darras, S., Granier, C., and Pérez García-Pando, C.: Copernicus Atmosphere Monitoring Service TEMPOral profiles (CAMS-TEMPO): global and European emission temporal profile maps for atmospheric chemistry modelling, Earth Syst. Sci. Data, 13, 367–404, https://doi.org/10.5194/essd-13-367-2021, 2021.

Guo, H., Xu, L., Bougiatioti, A., Cerully, K. M., Capps, S. L., Hite, J. R., Carlton, A. G., Lee, S.-H., Bergin, M. H., Ng, N. L., Nenes, A., and Weber, R. J.: Fine-particle water and pH in the southeastern United States, Atmospheric Chemistry and Physics, 15, 5211–5228, https://doi.org/10.5194/acp-15-5211-2015, 2015.

Guo, H., Sullivan, A. P., Campuzano-Jost, P., Schroder, J. C., Lopez-Hilfiker, F. D., Dibb, J. E., Jimenez, J. L., Thornton, J. A., Brown, S. S., Nenes, A., and Weber, R. J.: Fine particle pH and the partitioning of nitric acid during winter in the northeastern United States, Journal of Geophysical Research: Atmospheres, 121, 10,355-10,376, https://doi.org/10.1002/2016JD025311, 2016.

Guo, H., Liu, J., Froyd, K. D., Roberts, J. M., Veres, P. R., Hayes, P. L., Jimenez, J. L., Nenes, A., and Weber, R. J.: Fine particle pH and gas–particle phase partitioning of inorganic species in Pasadena, California, during the 2010 CalNex campaign, Atmospheric Chemistry and Physics, 17, 5703–5719, https://doi.org/10.5194/acp-17-5703-2017, 2017a.

Guo, H., Weber, R. J., and Nenes, A.: High levels of ammonia do not raise fine particle pH sufficiently to yield nitrogen oxide-dominated sulfate production, Scientific Reports, 7, 12109, https://doi.org/10.1038/s41598-017-11704-0, 2017b.

Guo, H., Nenes, A., and Weber, R. J.: The underappreciated role of nonvolatile cations in aerosol ammonium-sulfate molar ratios, Atmos. Chem. Phys, 18, 17307–17323, https://doi.org/10.5194/acp-18-17307-2018, 2018.

Hamer, P. D., Walker, S.-E., Sousa-Santos, G., Vogt, M., Vo-Thanh, D., Lopez-Aparicio, S., Schneider, P., Ramacher, M. O. P., and Karl, M.: The urban dispersion model EPISODE v10.0 – Part 1: An Eulerian and sub-grid-scale air quality model and its application in Nordic winter conditions, Geoscientific Model Development, 13, 4323–4353, https://doi.org/10.5194/gmd-13-4323-2020, 2020.

Harris, E., Sinha, B., Pinxteren, D. V., Tilgner, A., Fomba, K. W., Schneider, J., Roth, A., Gnauk, T., Fahlbusch, B., Mertes, S., Lee, T., Collett, J., Foley, S., Borrmann, S., Hoppe, P., and Herrmann, H.: Enhanced Role of Transition Metal, Science, 340, 727–730, https://doi.org/10.1126/science.1230911, 2013.

Hennigan, C. J., Izumi, J., Sullivan, A. P., Weber, R. J., and Nenes, A.: A critical evaluation of proxy methods used to estimate the acidity of atmospheric particles, Atmospheric Chemistry and Physics, 15, 2775–2790, https://doi.org/10.5194/acp-15-2775-2015, 2015.

Hurley, P. J., Physick, W. L., and Luhar, A. K.: TAPM: a practical approach to prognostic meteorological and air pollution modelling, Environmental Modelling & Software, 20, 737–752, https://doi.org/10.1016/j.envsoft.2004.04.006, 2005.

Im, U., Christodoulaki, S., Violaki, K., Zarmpas, P., Kocak, M., Daskalakis, N., Mihalopoulos, N., and Kanakidou, M.: Atmospheric deposition of nitrogen and sulfur over southern Europe with focus on the Mediterranean and the Black Sea, Atmospheric Environment, 81, https://doi.org/10.1016/j.atmosenv.2013.09.048, 2013.

Karl, M. and Ramacher, M. O. P.: Urban Atmospheric Chemistry with the EPISODE-CityChem Model, in: Air Pollution Modeling and its Application XXVII, edited by: Mensink, C. and Matthias, V., Springer Berlin Heidelberg, Berlin, Heidelberg, 235–239, https://doi.org/10.1007/978-3-662-63760-9_33, 2021.

Karl, M., Walker, S.-E., Solberg, S., and Ramacher, M. O. P.: The Eulerian urban dispersion model EPISODE – Part 2: Extensions to the source dispersion and photochemistry for EPISODE–CityChem v1.2 and its application to the city of Hamburg, Geoscientific Model Development, 12, 3357–3399, https://doi.org/10.5194/gmd-12-3357-2019, 2019.

Karl, M., Ramacher, M. O. P., Oppo, S., Lanzi, L., Majamäki, E., Jalkanen, J.-P., Lanzafame, G. M., Temime-Roussel, B., Le Berre, L., and D'Anna, B.: Measurement and Modeling of Ship-Related Ultrafine Particles and Secondary Organic Aerosols in a Mediterranean Port City, Toxics, 11, 771, https://doi.org/10.3390/toxics11090771, 2023.

Karydis, V. A., Tsimpidi, A. P., Pozzer, A., Astitha, M., and Lelieveld, J.: Effects of mineral dust on global atmospheric nitrate concentrations, Atmospheric Chemistry and Physics, 16, 1491–1509, https://doi.org/10.5194/acp-16-1491-2016, 2016.

Koçak, M., Kubilay, N., and Mihalopoulos, N.: Ionic composition of lower tropospheric aerosols at a Northeastern

20

Mediterranean site: implications regarding sources and long-range transport, Atmospheric Environment, 38, 2067–2077, https://doi.org/10.1016/j.atmosenv.2004.01.030, 2004.

Koçak, M., Theodosi, C., Zarmpas, P., Séguret, M. J. M., Herut, B., Kallos, G., Mihalopoulos, N., Kubilay, N., and Nimmo, M.: Influence of mineral dust transport on the chemical composition and physical properties of the Eastern Mediterranean aerosol, Atmospheric Environment, 57, 266–277, https://doi.org/10.1016/j.atmosenv.2012.04.006, 2012.

Kontos, S., Kakosimos, K., Liora, N., Poupkou, A., and Melas, D.: Towards a regional dust modeling system in the central Middle East: Evaluation, uncertainties and recommendations, Atmospheric Environment, 246, 118160, https://doi.org/10.1016/j.atmosenv.2020.118160, 2021.

Koulouri, E., Saarikoski, S., Theodosi, C., Markaki, Z., Gerasopoulos, E., Kouvarakis, G., Mäkelä, T., Hillamo, R., and Mihalopoulos, N.: Chemical composition and sources of fine and coarse aerosol particles in the Eastern Mediterranean, Atmospheric Environment, 42, 6542–6550, https://doi.org/10.1016/j.atmosenv.2008.04.010, 2008.

Kushta, J., Georgiou, G. K., Proestos, Y., Christoudias, T., Thunis, P., Savvides, C., Papadopoulos, C., and Lelieveld, J.: Evaluation of EU air quality standards through modeling and the FAIRMODE benchmarking methodology, Air Qual Atmos Health, 12, 73–86, https://doi.org/10.1007/s11869-018-0631-z, 2019.

Lasne, J., Lostier, A., Salameh, T., Athanasopoulou, E., Karagiannis, D., Kakouri, A., Vassaux, S., Lesueur, D., and Romanias, M. N.: NOx emissions by real-world fresh and old asphalt mixtures: Impact of temperature, relative humidity, and UV-irradiation, Urban Climate, 49, 101457, https://doi.org/10.1016/j.uclim.2023.101457, 2023.

Lawal, A. S., Guan, X., Liu, C., Henneman, L. R. F., Vasilakos, P., Bhogineni, V., Weber, R. J., Nenes, A., and Russell, A. G.: Linked Response of Aerosol Acidity and Ammonia to SO_2 and NO_x Emissions Reductions in the United States, Environmental Science & Technology, 52, 9861–9873, https://doi.org/10.1021/acs.est.8b00711, 2018.

Lee-Taylor, J. and Madronich, S.: Calculation of actinic fluxes with a coupled atmosphere–snow radiative transfer model, J.-Geophys.-Res., 107, https://doi.org/10.1029/2002JD002084, 2002.

Liakakou, E., Fourtziou, L., Paraskevopoulou, D., Speyer, O., Lianou, M., Grivas, G., Myriokefalitakis, S., and Mihalopoulos, N.: High-Resolution Measurements of SO2, HNO3 and HCl at the Urban Environment of Athens, Greece: Levels, Variability and Gas to Particle Partitioning, Atmosphere, 13, 218, https://doi.org/10.3390/atmos13020218, 2022.

Liakakou, E., Mihalopoulos, N., Theodosi, C., Tsiodra, E., Kaskaoutis, D. G., Koukouli, M.-E., Balis, D., Kharol, S. K., Shephard, M. W., Dammers, E., and Cady-Pereira, K. E.: Inorganic Aerosol Precursors in the Mediterranean Atmosphere, in: Atmospheric Chemistry in the Mediterranean Region: Volume 1 - Background Information and Pollutant Distribution, edited by: Dulac, F., Sauvage, S., and Hamonou, E., Springer International Publishing, Cham, 471–503, https://doi.org/10.1007/978-3-031-12741-0_14, 2023.

Liao, H., Adams, P. J., Chung, S. H., Seinfeld, J. H., Mickley, L. J., and Jacob, D. J.: Interactions between tropospheric chemistry and aerosols in a unified general circulation model, Journal of Geophysical Research, 108, 4001, https://doi.org/10.1029/2001JD001260, 2003.

Liora, N., Kontos, S., Parliari, D., Akritidis, D., Poupkou, A., Papanastasiou, D. K., and Melas, D.: "On-Line" Heating Emissions Based on WRF Meteorology—Application and Evaluation of a Modeling System over Greece, Atmosphere, 13, 568, https://doi.org/10.3390/atmos13040568, 2022.

Liu, M., Huang, X., Song, Y., Tang, J., Cao, J., Zhang, X., Zhang, Q., Wang, S., Xu, T., Kang, L., Cai, X., Zhang, H., Yang, F., Wang, H., Yu, J. Z., Lau, A. K. H., He, L., Huang, X., Duan, L., Ding, A., Xue, L., Gao, J., Liu, B., and Zhu, T.: Ammonia emission control in China would mitigate haze pollution and nitrogen deposition, but worsen acid rain, Proceedings of the National Academy of Sciences, 116, 7760–7765, https://doi.org/10.1073/pnas.1814880116, 2019.

Liu, T., Chan, A. W. H., and Abbatt, J. P. D.: Multiphase Oxidation of Sulfur Dioxide in Aerosol Particles: Implications for Sulfate Formation in Polluted Environments, https://doi.org/10.1021/acs.est.0c06496, 2021.

Mantas, E., Remoundaki, E., Halari, I., Kassomenos, P., Theodosi, C., Hatzikioseyian, A., and Mihalopoulos, N.: Mass closure and source apportionment of PM2.5 by Positive Matrix Factorization analysis in urban Mediterranean environment, Atmospheric Environment, 94, 154–163, https://doi.org/10.1016/j.atmosenv.2014.05.002, 2014.

Myhre, G., Shindell, D., Pongratz, J., and Stocker, T.: Anthropogenic and Natural Radiative Forcing, edited by: Stocker, T., Ludwig-Maximilians-Universität München, Cambridge, 659–740, https://doi.org/10.1017/CBO9781107415324.018, 2014.

Myriokefalitakis, S., Daskalakis, N., Gkouvousis, A., Hilboll, A., van Noije, T., Williams, J. E., Le Sager, P., Huijnen, V., Houweling, S., Bergman, T., Nüß, J. R., Vrekoussis, M., Kanakidou, M., and Krol, M. C.: Description and evaluation of a detailed gas-phase chemistry scheme in the TM5-MP global chemistry transport model (r112), Geoscientific Model

Development, 13, 5507–5548, https://doi.org/10.5194/gmd-13-5507-2020, 2020.

Myriokefalitakis, S., Bergas-Massó, E., Gonçalves-Ageitos, M., Pérez García-Pando, C., van Noije, T., Le Sager, P., Ito, A., Athanasopoulou, E., Nenes, A., Kanakidou, M., Krol, M. C., and Gerasopoulos, E.: Multiphase processes in the EC-Earth model and their relevance to the atmospheric oxalate, sulfate, and iron cycles, Geoscientific Model Development, 15, 3079–3120, https://doi.org/10.5194/gmd-15-3079-2022, 2022.

Nenes, A., Pandis, S. N., and Pilinis, C.: ISORROPIA: A New Thermodynamic Equilibrium Model for Multiphase Multicomponent Inorganic Aerosols, Aquatic Geochemistry, 4, 123–152, https://doi.org/10.1023/A:1009604003981, 1998.

Nenes, A., Pandis, S. N., Weber, R. J., and Russell, A.: Aerosol pH and liquid water content determine when particulate matter is sensitive to ammonia and nitrate availability, Atmospheric Chemistry and Physics, 20, 3249–3258, https://doi.org/10.5194/acp-20-3249-2020, 2020.

Ng, N. L., Herndon, S. C., Trimborn, A., Canagaratna, M. R., Croteau, P. L., Onasch, T. B., Sueper, D., Worsnop, D. R., Zhang, Q., Sun, Y. L., and Jayne, J. T.: An Aerosol Chemical Speciation Monitor (ACSM) for Routine Monitoring of the Composition and Mass Concentrations of Ambient Aerosol, Aerosol Science and Technology, 45, 780–794, https://doi.org/10.1080/02786826.2011.560211, 2011.

Ozga, I., Bonazza, A., Ait Lyazidi, S., Haddad, M., Ben-Ncer, A., Ghedini, N., and Sabbioni, C.: Pollution impact on the ancient ramparts of the Moroccan city Salé, Journal of Cultural Heritage, 14, S25–S33, https://doi.org/10.1016/j.culher.2012.10.018, 2013.

Panopoulou, A., Liakakou, E., Sauvage, S., Gros, V., Locoge, N., Stavroulas, I., Bonsang, B., Gerasopoulos, E., and Mihalopoulos, N.: Yearlong measurements of monoterpenes and isoprene in a Mediterranean city (Athens): Natural vs anthropogenic origin, Atmospheric Environment, 243, 117803, https://doi.org/10.1016/j.atmosenv.2020.117803, 2020.

Paraskevopoulou, D., Liakakou, E., Gerasopoulos, E., Theodosi, C., and Mihalopoulos, N.: Long-term characterization of organic and elemental carbon in the PM2.5 fraction: the case of Athens, Greece, Atmos. Chem. Phys., 14, 13313–13325, https://doi.org/10.5194/acp-14-13313-2014, 2014.

Paraskevopoulou, D., Liakakou, E., Gerasopoulos, E., and Mihalopoulos, N.: Sources of atmospheric aerosol from long-term measurements (5years) of chemical composition in Athens, Greece, Science of The Total Environment, 527–528, 165–178, https://doi.org/10.1016/j.scitotenv.2015.04.022, 2015.

Pope, C. A., Coleman, N., Pond, Z. A., and Burnett, R. T.: Fine particulate air pollution and human mortality: 25+ years of cohort studies, Environmental Research, 183, 108924, https://doi.org/10.1016/j.envres.2019.108924, 2020.

Pringle, K. J., Tost, H., Metzger, S., Steil, B., Giannadaki, D., Nenes, A., Fountoukis, C., Stier, P., Vignati, E., and Lelieveld, J.: Description and evaluation of GMXe: a new aerosol submodel for global simulations (v1), Geoscientific Model Development, 3, 413–413, https://doi.org/10.5194/gmd-3-413-2010, 2010.

Pye, H. O. T., Nenes, A., Alexander, B., Ault, A. P., Barth, M. C., Clegg, S. L., Collett, J. L., Fahey, K. M., Hennigan, C. J., Herrmann, H., Kanakidou, M., Kelly, J. T., Ku, I. T., Faye McNeill, V., Riemer, N., Schaefer, T., Shi, G., Tilgner, A., Walker, J. T., Wang, T., Weber, R., Xing, J., Zaveri, R. A., and Zuend, A.: The acidity of atmospheric particles and clouds, Atmospheric Chemistry and Physics, 20, 4809–4888, https://doi.org/10.5194/acp-20-4809-2020, 2020.

Ramacher, M. O. P., Kakouri, A., Speyer, O., Feldner, J., Karl, M., Timmermans, R., Denier van der Gon, H., Kuenen, J., Gerasopoulos, E., and Athanasopoulou, E.: The UrbEm Hybrid Method to Derive High-Resolution Emissions for City-Scale Air Quality Modeling, Atmosphere, 12, 1404, https://doi.org/10.3390/atmos12111404, 2021.

Salter, M. E., Zieger, P., Acosta Navarro, J. C., Grythe, H., Kirkevåg, A., Rosati, B., Riipinen, I., and Nilsson, E. D.: An empirically derived inorganic sea spray source function incorporating sea surface temperature, Atmospheric Chemistry and Physics, 15, 11047–11066, https://doi.org/10.5194/acp-15-11047-2015, 2015.

Sander, R.: Compilation of Henry's law constants (version 4.0) for water as solvent, Atmospheric Chemistry and Physics, 15, 4399–4981, https://doi.org/10.5194/acp-15-4399-2015, 2015.

Sandu, A. and Sander, R.: Technical note: Simulating chemical systems in Fortran90 and Matlab with the Kinetic PreProcessor KPP-2.1, Atmospheric Chemistry and Physics, 6, 187–195, https://doi.org/10.5194/acp-6-187-2006, 2006.

Santiago, J. L., Rivas, E., Gamarra, A. R., Vivanco, M. G., Buccolieri, R., Martilli, A., Lechón, Y., and Martín, F.: Estimates of population exposure to atmospheric pollution and health-related externalities in a real city: The impact of spatial resolution on the accuracy of results, Science of The Total Environment, 819, 152062, https://doi.org/10.1016/j.scitotenv.2021.152062, 2022.

Sarnat, S. E., Winquist, A., Schauer, J. J., Turner, J. R., and Sarnat, J. A.: Fine Particulate Matter Components and

97   Emergency Department Visits for Cardiovascular and Respiratory Diseases in the St. Louis, Missouri–Illinois, Metropolitan
98   Area, Environ Health Perspect, 123, 437–444, https://doi.org/10.1289/ehp.1307776, 2015.
99   Sciare, J., Oikonomou, K., Cachier, H., Mihalopoulos, N., Andreae, M. O., Maenhaut, W., and Sarda-Estève, R.: Aerosol
00   mass closure and reconstruction of the light scattering coefficient over the Eastern Mediterranean Sea during the MINOS
01   campaign, Atmospheric Chemistry and Physics, 5, 2253–2265, https://doi.org/10.5194/acp-5-2253-2005, 2005.
02   Seinfeld, J. H. and Pandis, S. N.: Atmospheric Chemistry and Physics: From Air Pollution to Climate Change, 2006.
03   Slørdal, L. H., McInnes, H., and Krognes, T.: The Air Quality Management System AirQUIS, in: Information Technologies
04   in Environmental Engineering, Berlin, Heidelberg, 21–33, https://doi.org/10.1007/978-3-540-71335-7_6, 2007.
05   Sokhi, R. S., Moussiopoulos, N., Baklanov, A., Bartzis, J., Coll, I., Finardi, S., Friedrich, R., Geels, C., Grönholm, T.,
06   Halenka, T., Ketzel, M., Maragkidou, A., Matthias, V., Moldanova, J., Ntziachristos, L., Schäfer, K., Suppan, P., Tsegas, G.,
07   Carmichael, G., Franco, V., Hanna, S., Jalkanen, J.-P., Velders, G. J. M., and Kukkonen, J.: Advances in air quality research
08   – current and emerging challenges, Atmos. Chem. Phys., 22, 4615–4703, https://doi.org/10.5194/acp-22-4615-2022, 2022.
09   Sposito, G.: The Chemistry of Soils, Oxford University Press, Oxford, 277 pp., 1989.
10   Stavroulas, I., Bougiatioti, A., Grivas, G., Paraskevopoulou, D., Tsagkaraki, M., Zarmpas, P., Liakakou, E., Gerasopoulos,
11   E., and Mihalopoulos, N.: Sources and processes that control the submicron organic aerosol composition in an urban
12   Mediterranean environment (Athens): a high temporal-resolution chemical composition measurement study, Atmospheric
13   Chemistry and Physics, 19, 901–919, https://doi.org/10.5194/acp-19-901-2019, 2019.
14   Stavroulas, I., Grivas, G., Liakakou, E., Kalkavouras, P., Bougiatioti, A., Kaskaoutis, D. G., Lianou, M., Papoutsidaki, K.,
15   Tsagkaraki, M., Zarmpas, P., Gerasopoulos, E., and Mihalopoulos, N.: Online Chemical Characterization and Sources of
16   Submicron Aerosol in the Major Mediterranean Port City of Piraeus, Greece, Atmosphere, 12, 1686,
17   https://doi.org/10.3390/atmos12121686, 2021.
18   Theodosi, C., Tsagkaraki, M., Zarmpas, P., Grivas, G., Liakakou, E., Paraskevopoulou, D., Lianou, M., Gerasopoulos, E.,
19   and Mihalopoulos, N.: Multi-year chemical composition of the fine-aerosol fraction in Athens, Greece, with emphasis on the
20   contribution of residential heating in wintertime, Atmospheric Chemistry and Physics, 18, 14371–14391,
21   https://doi.org/10.5194/acp-18-14371-2018, 2018.
22   Vignati, E., Facchini, M. C., Rinaldi, M., Scannell, C., Ceburnis, D., Sciare, J., Kanakidou, M., Myriokefalitakis, S.,
23   Dentener, F., and ODowd, C. D.: Global scale emission and distribution of sea-spray aerosol: Sea-salt and organic
24   enrichment, Atmospheric Environment, 44, 670–677, https://doi.org/10.1016/j.atmosenv.2009.11.013, 2010.
25   Wang, T., Liu, Y., Cheng, H., Wang, Z., Fu, H., Chen, J., and Zhang, L.: Significant formation of sulfate aerosols
26   contributed by the heterogeneous drivers of dust surface, Atmospheric Chemistry and Physics, 22, 13467–13493,
27   https://doi.org/10.5194/acp-22-13467-2022, 2022.
28   Watmough, S. A., Eimers, C., and Baker, S.: Impediments to recovery from acid deposition, Atmospheric Environment, 146,
29   15–27, https://doi.org/10.1016/j.atmosenv.2016.03.021, 2016.
30   WHO: WHO global air quality guidelines: particulate matter (PM2.5 and PM10), ozone, nitrogen dioxide, sulfur dioxide and
31   carbon monoxide, , xxi, 273 p., 2021.
32   Williams, J. E., van Velthoven, P. F. J., and Brenninkmeijer, C. A. M.: Quantifying the uncertainty in simulating global
33   tropospheric composition due to the variability in global emission estimates of Biogenic Volatile Organic Compounds,
34   Atmospheric Chemistry and Physics, 13, 2857–2891, https://doi.org/10.5194/acp-13-2857-2013, 2013.
35   Williams, J. E., Boersma, K. F., Le Sager, P., and Verstraeten, W. W.: The high-resolution version of TM5-MP for
36   optimized satellite retrievals: description and validation, Geoscientific Model Development, 10, 721–750,
37   https://doi.org/10.5194/gmd-10-721-2017, 2017.
38   Yarwood, G., Rao, S., and Yocke, M.: Updates to the carbon bond chemical mechanism: CB05 - Prepared for Deborah
39   Luecken U.S. Environmental Protection Agency Research Triangle Park, NC 27703, YOCKE AND COMPANY, 2005.
40   Zakoura, M. and Pandis, S. N.: Overprediction of aerosol nitrate by chemical transport models: The role of grid resolution,
41   Atmospheric Environment, 187, 390–400, https://doi.org/10.1016/j.atmosenv.2018.05.066, 2018.
42   Zhang, L., Wang, T., Zhang, Q., Zheng, J., Xu, Z., and Lv, M.: Potential sources of nitrous acid (HONO) and their impacts
43   on ozone: A WRF-Chem study in a polluted subtropical region: MODELING HONO IN A SUBTROPICAL REGION, J.
44   Geophys. Res. Atmos., 121, 3645–3662, https://doi.org/10.1002/2015JD024468, 2016.
45   Zhang, Y., Yang, Y., Zhang, L., Xu, H., Sun, J., Wang, T., Li, F., Chang, X., Ho, S. S. H., Li, B., Wang, B., Cao, J., and
46   Shen, Z.: Insight into the contributions of primary emissions of sulfate, nitrate, and ammonium from residential solid fuels to

23

ambient PM2.5, Atmospheric Research, 290, 106790, https://doi.org/10.1016/j.atmosres.2023.106790, 2023.

Zhang, Z., Gao, J., Engling, G., Tao, J., Chai, F., Zhang, L., Zhang, R., Sang, X., Chan, C., Lin, Z., and Cao, J.: Characteristics and applications of size-segregated biomass burning tracers in China's Pearl River Delta region, Atmospheric Environment, 102, 290–301, https://doi.org/10.1016/j.atmosenv.2014.12.009, 2015.

Zhang, Z.-H., Hartner, E., Utinger, B., Gfeller, B., Paul, A., Sklorz, M., Czech, H., Yang, B. X., Su, X. Y., Jakobi, G., Orasche, J., Schnelle-Kreis, J., Jeong, S., Gröger, T., Pardo, M., Hohaus, T., Adam, T., Kiendler-Scharr, A., Rudich, Y., Zimmermann, R., and Kalberer, M.: Are reactive oxygen species (ROS) a suitable metric to predict toxicity of carbonaceous aerosol particles?, Atmospheric Chemistry and Physics, 22, 1793–1809, https://doi.org/10.5194/acp-22-1793-2022, 2022.

Code and data availability. The source codes of the EPISODE-CityChem model version 1.8 and the preprocessing utilities are accessible in the release under the RPL license at https://doi.org/10.5281/zenodo.8063985. The thermodynamic equilibrium model ISORROPIA II is available at https://www.epfl.ch/labs/lapi/software/isorropia/.

Tables and Figures

Table 1. Reaction rates and constants used in EPISODE-CityChem for this study.

Reaction	Rate	Reference
	Gas-phase chemistry rates ($cm^3\ mol^{-1}\ s^{-1}$)	
$SO_2(g) + OH(g) \rightarrow H_2SO_4(g) + HO_2(g)$	$k_0 = 2.8 \times 10^{-31}(T/300)^{-2.6} \times [N_2]$ $k_\infty = 2.0 \times 10^{-12}$ $F_c = 0.75$	1
	Aqueous-phase chemistry rates ($l\ mol^{-1}\ s^{-1}$)	
$HSO_3^- + H_2O_2\ (+ H^+) \rightarrow H_2SO_4(aq) + O_2(aq)$	$7.5 \times 10^7\ e^{-4430(1/T\ -\ 1/298)} \times [H^+]/(1 + 13.0 \times [H^+])$	2
$SO_2(aq) + O_3(aq)\ (+ H_2O) \rightarrow S(VI)$	2.4×10^4	
$HSO_3^- + O_3 \rightarrow HSO_4^- + O_2(aq)$	$3.7 \times 10^5\ e^{-5530(1/T\ -\ 1/298)}$	2
$SO_3^{2-} + O_3 \rightarrow SO_4^{2-} + O_2(aq)$	$1.5 \times 10^9\ e^{-5280(1/T\ -\ 1/298)}$	2
	Dissociation constants ($mol\ l^{-1}$)	
$SO_2(aq) \leftrightarrow SO_3^- + H^+$	$1.3 \times 10^{-2}\ e^{1960(1/T\ -\ 1/298)}$	2
$SO_3^- \leftrightarrow SO_3^{2-} + H^+$	$6.6 \times 10^{-8}\ e^{1500(1/T\ -\ 1/298)}$	2
$NH_3(aq) \leftrightarrow NH_4^+ + HO^-$	$1.7 \times 10^{-5}\ e^{-450(1/T\ -\ 1/298)}$	2
$CO_2(aq) \leftrightarrow HCO_3^- + H^+$	$4.3 \times 10^{-7}\ e^{-1000(1/T\ -\ 1/298)}$	2
$HCO_3^- \leftrightarrow CO_3^{2-} + H^+$	$4.68 \times 10^{-11}\ e^{-1760(1/T\ -\ 1/298)}$	2
	Henry law constants ($mol\ m^{-3}\ Pa^{-1}$)	
SO_2	$1.3 \times 10^{-2}\ e^{2900(1/T\ -\ 1/298)}$	3
H_2O_2	$9.1 \times 10^2\ e^{6600(1/T\ -\ 1/298)}$	3
O_3	$1.0 \times 10^{-4}\ e^{2800(1/T\ -\ 1/298)}$	3
CO_2	$3.3 \times 10^{-4}\ e^{2400(1/T\ -\ 1/298)}$	3
NH_3	$5.9 \times 10^{-1}\ e^{4200(1/T\ -\ 1/298)}$	3
	Heterogeneous chemistry	
$SO_2(g)\ \{+ Dust\} \rightarrow H_2SO_4$	$\gamma = 1.0 \times 10^{-1}$ (RH>50%) $\gamma = 3.0 \times 10^{-1}$ (RH<50%)	4

283 [1] (Atkinson et al., 2004); [2] (Seinfeld and Pandis, 2006); [3] (Sander, 2015); [4] (Liao et al., 2003)
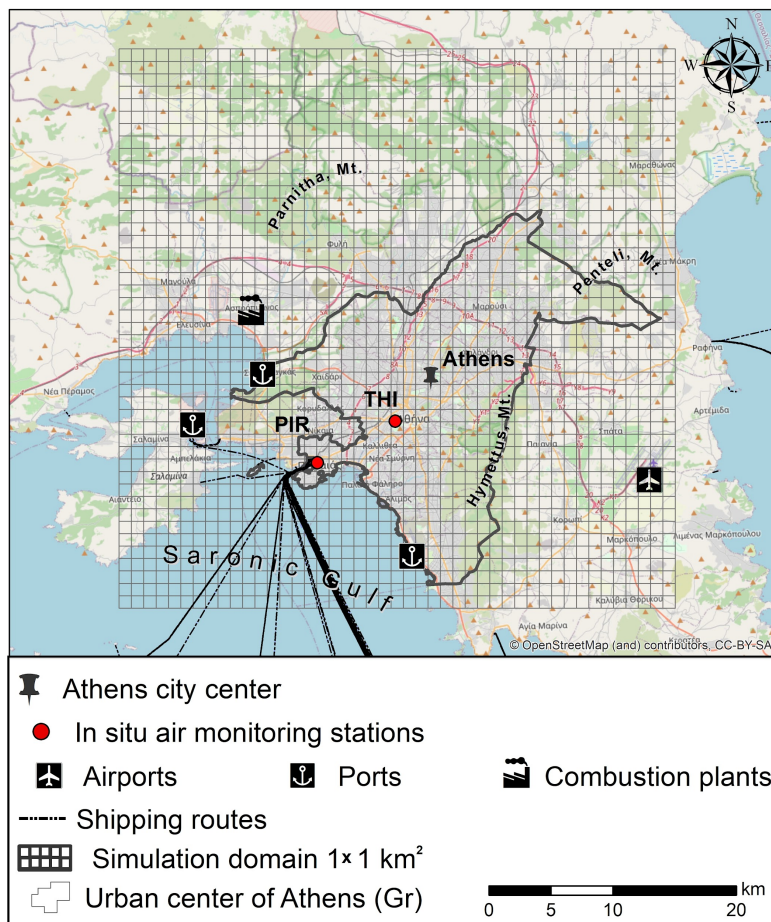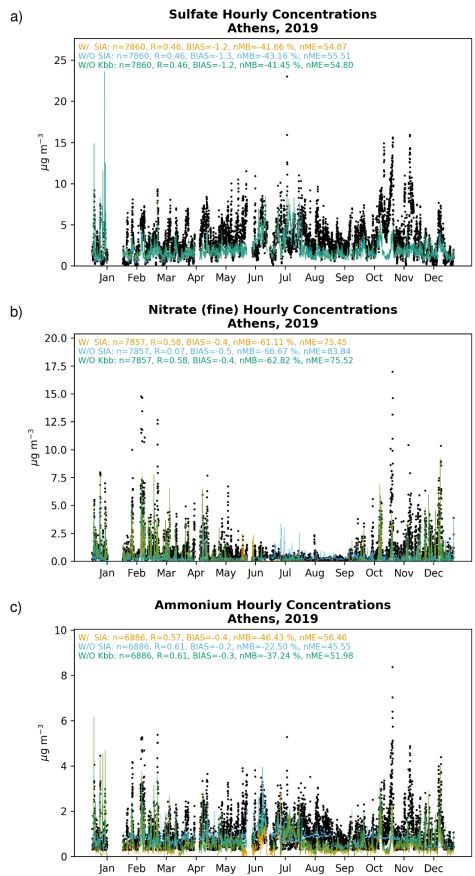284

Figure 1. Model domain of the Greater Area of Athens, Greece. The gridded rectangles correspond to the air quality simulation domains. Sites (red dots) correspond to the air quality measurement stations during the simulation periods.

a) Sulfate Hourly Concentrations
Athens, 2019

b) Nitrate (fine) Hourly Concentrations
Athens, 2019

c) Ammonium Hourly Concentrations
Athens, 2019

89

Figure 2: Comparison (µg m⁻³) of hourly mean observations (black dots) in Piraeus (1-16 January 2019; 11 June - 9 July 2019) and in Thissio (17 January - 10 June 2019; 10 July - 31 December 2019) for a) sulfate, b) fine nitrate, and c) ammonium, to the EPISODE-CityChem simulations for base case simulation (W/ SIA; orange line), without considering SIA formation (W/O SIA; blue line) and without considering the contribution of K⁺ from domestic heating processes in thermodynamic calculations (W/O Kbb; green line). The respective correlation statistics are also provided.

95

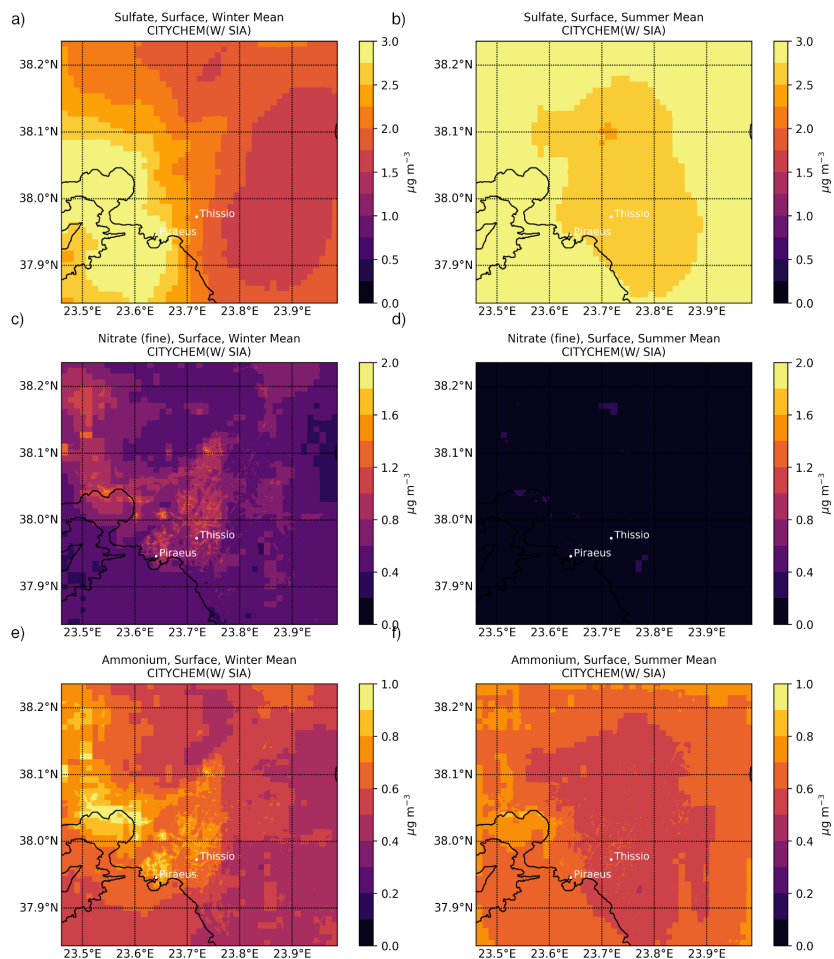**Figure 3: Surface concentrations (µg m⁻³) over the Greater Area of Athens of sulfate (a,b), nitrate (c,d), and ammonium (e,f), as simulated by EPISODE-CityChem on a horizontal resolution of 100 x 100 m² for winter (December, January, and February; a,c,e) and summer (June, July, and August; b,d,f) of the year 2019.**
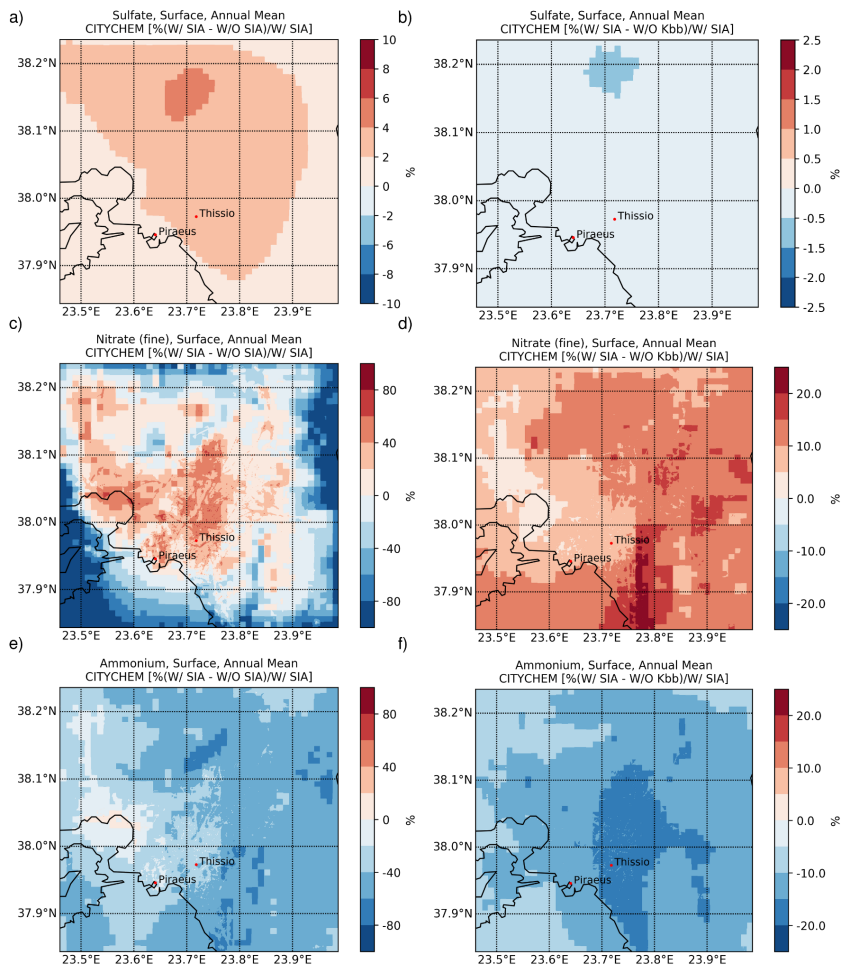
28

Figure 4: Annual mean percentage (%) contribution of secondary formation processes to the surface concentrations of sulfate (a), nitrate (c), and ammonium (e), and the respective impact of including the K^+ from domestic burning in thermodynamic calculations (b,d,f), as simulated by EPISODE-CityChem on a horizontal resolution of 100 x 100 m^2 over the Greater Area of Athens for the year 2019.
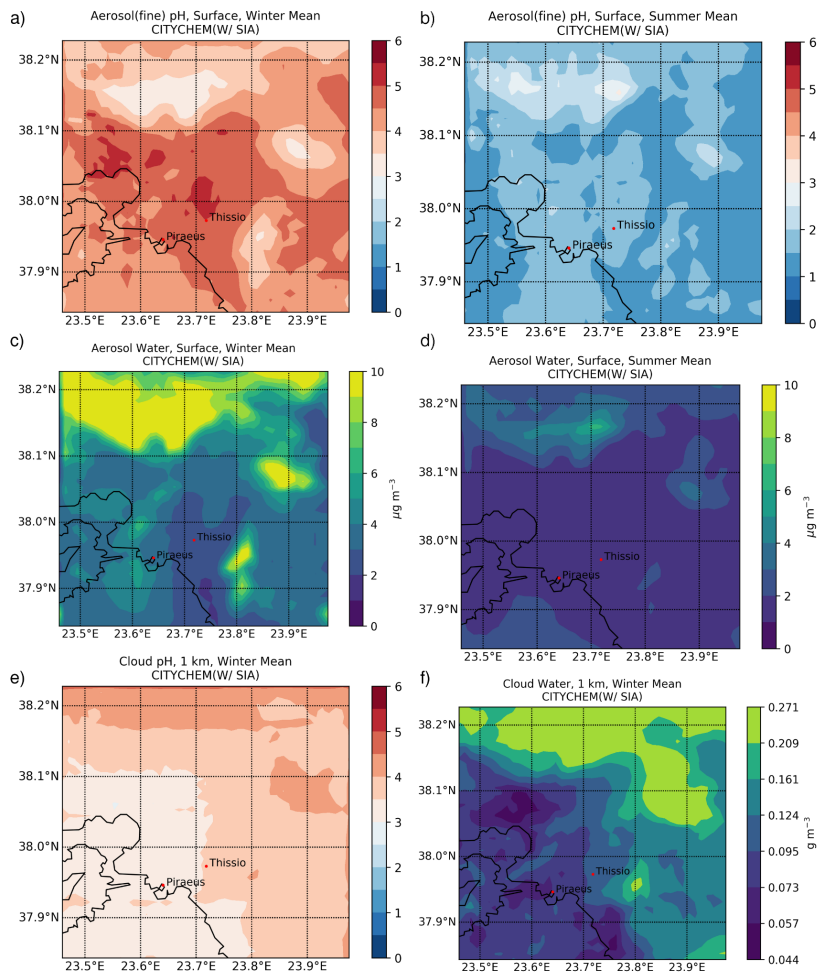
29

Figure 5: Surface fine aerosol pH (a,b) and aerosol water content (c,d; μg m⁻³) for winter (December, January, February; a,c) and summer (June, July, August; b,d) 2019, along with the cloud pH at 1 km altitude for winter (e) as simulated by EPISODE-CityChem on a horizontal resolution of 1 x 1 km² over the Greater Area of Athens. The respective cloud water content (g m⁻³) is also presented (g).

30